



GEOLOGY FOR SOCIETY

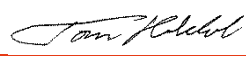
SINCE 1858



**GEOLOGICAL
SURVEY OF
NORWAY**

· NGU ·



Report no.: 2015.006		ISSN: 0800-3416 (print) ISSN: 2387-3515 (online)		Grading: Open	
Title: Mapping of marine clay layers using airborne EM and ground geophysical methods at Byneset, Trondheim municipality					
Authors: Vikas C. Baranwal, Jan S. Rønning, Einar Dalsegg, Inger-Lise Solberg, Jan Fr. Tønnesen, Alexei Rodionov & Håvard Dretvik,			Client: NGU		
County: Sør Trøndelag			Commune: Trondheim		
Map-sheet name (M=1:250.000) Trondheim			Map-sheet no. and -name (M=1:50.000) 1521 I Orkanger		
Deposit name and grid-reference: UTM 32 N			Number of pages: 59		Price (NOK): 150,-
Fieldwork carried out: June – Nov. 2013			Date of report: 22.02.2015		Map enclosures:
Fieldwork carried out: June – Nov. 2013		Date of report: 22.02.2015		Project no.: 348400	Person responsible: 
Summary: Airborne and ground geophysical surveys were performed at Byneset, Trondheim in Autumn 2013. On 1 st January, 2012 a landslide occurred in the centre of the area. Main aim for these surveys was to see usefulness of Frequency-domain Helicopter-borne ElectroMagnetic (FHEM) data in mapping of the clay layers/marine sediments and cross-check it with 2D resistivity and refraction seismic. The survey area was also visually inspected to detect exposed or very shallow bedrock. 2D resistivity and refraction seismic surveys were performed along parts of the FHEM lines. Two 1D codes from University of British Columbia (UBC) and Aarhus University are used to invert FHEM data. Aarhus software is found more appropriate and up-to-date to invert FHEM data with many additional features which UBC software does not offer e.g. laterally and specially constrained inversion, depth of investigation (doi) calculation etc. DOI calculated from Aarhus software suggests that only models down to approx. 40 to 150 m depth below the surface are reliable from FHEM data depending on the background resistivity in the area. Interpretation of FHEM data shows correlation with 2D resistivity and refraction seismic data. Comparison of FHEM interpretation together with 2D resistivity, refraction seismic interpretation and exposed bedrock locations suggests that FHEM data can be used for clay layer mapping and to indicate a rough bedrock depth. It can differentiate between layers of unleached marine clay (< 10 Ωm) and leached marine clay or possible quick clay (10-100 Ωm). However, similar resistivity values of possible quick clay (10-100 Ωm) can also suggest non-quick, leached clay and silty sediments. FHEM inversion suggests bedrock resistivity as low as 50 Ωm which should be actually several thousand Ωm. Graphite bearing bedrock could be one of the reasons for low resistivity of the bedrock. It is observed that depth to bedrock below a conductive layer of 30 m or more are not reliable in clay areas, and the interpretation of resistivity values from FHEM data below such conductive layers may be incorrect. A bedrock depth map is produced for resistive zone > 200 Ωm which has shown correlation with observed bedrock locations and bedrock depth observed from drilling at few locations. However, such a bedrock depth map deduced from FHEM data alone is not very accurate. Borehole data are generally used to adapt it to the ground truth. FHEM resistivity from few locations close to geotechnical drilling is also compared with resistivity from RCPTu and 2D resistivity survey and found in good agreement. An interpretation of geological, geophysical and geotechnical data from the area is presented in another report (Solberg et al. 2015).					
Keywords		Frequency domain EM		Helicopterborne	
2D resistivity		Refraction seismic		Inversion	
Land slide		Quick clay		Scientific report	

Content

- 1. INTRODUCTION..... 11
- 2. LOCATON AND SURVEY SPECIFICATION..... 12
 - 2.1 Location of geotechnical drilling and bedrock sampling 12
 - 2.2 Ground geophysical survey parameters..... 14
 - 2.2.1 2D Resistivity survey 14
 - 2.2.2 Refraction seismic survey 14
 - 2.3 Airborne Survey Parameters..... 14
 - 2.3.1 Airborne Survey Instrumentation..... 15
 - 2.3.2 Calibration..... 16
- 3. DATA PROCESSING AND RESULTS 17
 - 3.1 Ground geophysical surveys..... 17
 - 3.1.1 Refraction seismic survey 17
 - 3.1.2 2D Resistivity survey 18
 - 3.2 Processing of FHEM Data..... 20
 - 3.3 1D Inversion of FHEM data 27
 - 3.3.1 UBC’s 1D code: EM1DFM..... 27
 - 3.3.2 Aarhus Constrained 1D inversion: AarhusInv 32
 - 3.3.3 Comparison of inverted 2D resistivity and FHEM models..... 35
 - 3.4 3D presentation of inverted data..... 41
 - 3.4.1 Stacked profiles and horizontal slices 41
 - 3.4.2 Depth to bedrock 45
 - 3.4.3 Comparison of resistivity data towards the depth 50
- 4. DISCUSSION 54
 - 4.1 Evaluation of inversion codes for FHEM data 54
 - 4.2 Inverted resistivity levels from 2D resistivity and FHEM data..... 54
 - 4.3 Depth to bedrock from FHEM survey 55
 - 4.4 Mapping efficiency of airborne survey over ground survey 55
- 5. CONCLUSIONS..... 56
- 6. REFERENCES..... 57

FIGURES

Figure 1: Quaternary geological map of the survey area and profiles of the geophysical surveys. See text for details.....	13
Figure 2: Classification of sediments based on resistivity values obtained from interpretation of 2D resistivity measurements in different projects (from Solberg et al. 2008).	14
Figure 3: Hummingbird system in the air during a survey.....	16
Figure 4: (a) Legend used in refraction seismic interpretation.....	17
Figure 4: (b) Refraction seismic interpretation along line -8.	18
Figure 5: Refraction seismic interpretation along line 142.	18
Figure 6: Refraction seismic interpretation along line 272.	18
Figure 7: Inverted model from 2D resistivity data along line -8. Dashed black lines show seismic velocity boundaries and dashed red line shows topography of seismic profile. Lower dashed black line represents interpreted bedrock depth.....	19
Figure 8: Inverted model from 2D resistivity data along line 142. Dashed black lines show seismic velocity layers and dashed red line shows topography of seismic profile. Lower dashed black line represents interpreted bedrock depth.....	19
Figure 9: Inverted model from 2D resistivity data along line 272. Dashed black lines show seismic velocity layers and dashed red line shows topography of seismic profile. Lower dashed black line represents interpreted bedrock depth.....	20
Figure 10: Inverted model from 2D resistivity data along line 551. There was no seismic line along this profile.	20
Figure 11: Homogeneous half-space inversion of FHEM data at frequency 34 kHz coplanar coils. Exposed bedrock locations are marked by black dots.	22
Figure 12: Homogeneous half-space inversion of FHEM data at frequency 7 kHz coaxial coils. Exposed bedrock locations are marked by black dots.	23
Figure 13: Homogeneous half-space inversion of FHEM data at frequency 6.6 kHz coplanar coils. Exposed bedrock locations are marked by black dots.	24
Figure 14: Homogeneous half-space inversion of FHEM data at frequency 980 Hz coaxial coils. Exposed bedrock locations are marked by black dots.	25
Figure 15: Homogeneous half-space inversion of FHEM data at frequency 880 Hz coplanar coils. Exposed bedrock locations are marked by black dots.	26
Figure 16 : Inverted model from five frequencies FHEM data along line -8 using UBC code with a starting model of 100 Ω m. Thicker dashed black lines show seismic velocity boundaries and dashed red line shows topography of seismic profile. Thinner dashed black line shows length and position of 2D resistivity survey profile.....	28
Figure 17: Fitting between measured FHEM data and computed data from inverted model obtained by UBC code along line -8. Symbols and solid lines represent measured and computed data for various frequencies, respectively.	28

Figure 18: Inverted model from five frequencies FHEM data along line 142 using UBC code with a starting model of 100 Ω m. Thicker dashed black lines show seismic velocity boundaries and dashed red line shows topography of seismic profile. Thinner dashed black line shows length and position of 2D resistivity survey profile.....	29
Figure 19: Fitting between measured FHEM data and computed data from inverted model obtained by UBC code along line 142. Symbols and solid lines represent measured and computed data for various frequencies, respectively.	29
Figure 20: Inverted model from five frequencies FHEM data along line 272 using UBC code with a starting model of 100 Ω m. Thicker dashed black lines show seismic velocity boundaries and dashed red line shows topography of seismic profile. Thinner dashed black line shows length and position of 2D resistivity survey profile.....	30
Figure 21: Fitting between measured FHEM data and computed data from inverted model obtained by UBC code along line 272. Symbols and solid lines represent measured and computed data for various frequencies, respectively.	30
Figure 22: Inverted model from five frequencies FHEM data along line 551 using UBC code with a starting model of 100 Ω m. Dashed black line shows length and position of 2D resistivity survey profile.....	31
Figure 23: Fitting between measured FHEM data and computed data from inverted model obtained by UBC code along line 551. Symbols and solid lines represent measured and computed data for various frequencies, respectively.	31
Figure 24: Inverted model from five frequencies FHEM data along line -8 using LCI of Aarhus code with a starting model of 10 Ω m. Green and purple line/symbols represent measured and computed altitude, respectively. Red line/symbol represents data residual. Fading of the image is done to show depth of investigation (DOI).	33
Figure 25: Inverted model from five frequencies FHEM data along line -8 using LCI of Aarhus code with a starting model of 10 Ω m (same as shown in Fig. 24 however plotted in Matlab). Thicker dashed black lines show seismic velocity boundaries and dashed red line shows topography of seismic profile. Thinner dashed black line shows length and position of 2D resistivity survey profile.	33
Figure 26: Fitting between measured FHEM data and computed data from inverted model obtained by LCI of Aarhus code along line -8 with a starting model of 10 Ω m. Symbols and solid lines represent measured and computed data for various frequencies, respectively.	34
Figure 27: Inverted model from five frequencies FHEM data along line -8 using LCI of Aarhus code with a starting model of 100 Ω m and with different settings. Thicker dashed black lines show seismic velocity boundaries and dashed red line shows topography of seismic profile. Thinner dashed black line shows length and position of 2D resistivity survey profile.....	34
Figure 28: Fitting between measured FHEM data and computed data from inverted model obtained by LCI of Aarhus code along line -8 with a starting model of 100 Ω m. Symbols and solid lines represent measured and computed data for various frequencies, respectively.	35
Figure 29: (a) Inversion results from 2D resistivity data, (b) FHEM data using UBC code, and (c) inverted model from five frequencies FHEM data along line -8 using LCI of Aarhus code with a starting model of 100 Ω m. Thicker dashed black lines show seismic velocity boundaries and dashed red line shows topography of seismic profile. Thinner dashed black line shows length and position of 2D resistivity survey profile.....	36
Figure 30: (a) Inversion results from 2D resistivity data, (b) FHEM data using UBC code and (c) inverted model from five frequencies FHEM data along line 142 using LCI of Aarhus code with a starting model of 100 Ω m. Thicker dashed black lines show seismic velocity boundaries and dashed red line shows topography of seismic profile. Thinner dashed black line shows length and position of 2D resistivity survey profile.	37

Figure 31: (a) Inversion results from 2D resistivity data, (b) FHEM data using UBC and (c) inverted model from five frequencies FHEM data code along line 272 using LCI of Aarhus code with a starting model of 100 Ωm . Thicker dashed black lines show seismic velocity boundaries and dashed red line shows topography of seismic profile. Thinner dashed black line shows length and position of 2D resistivity survey profile. 39

Figure 32: (a) Inversion results from 2D resistivity data, (b) FHEM data using UBC code and (c) inverted model from five frequencies FHEM data along line 551 using LCI of Aarhus code with a starting model of 100 Ωm . Dashed black line shows extent of 2D resistivity survey profile. Dashed black line shows length and position of 2D resistivity survey profile. 40

Figure 33: 3D resistivity image plot in Matlab from inversion of FHEM data. Inverted resistivity was obtained using SCI inversion of AarhusInv code with a starting model of 10 Ωm 42

Figure 34: 3D slices of resistivity image from 0 m to 30 m depth below surface plotted in Geosoft and extracted from inversion of FHEM data as shown in Fig. 33. 43

Figure 35: Resistivity image at 1 m depth obtained by SCI inversion of FHEM data with a starting model of 10 Ωm (from same image shown in Fig. 33). Black dots and black triangles represent exposed bedrock and geotechnical drilling locations, respectively. Red and blue lines represent 2D resistivity and seismic refraction profiles, respectively. 44

Figure 36: Depth of a resistivity zone $> 100 \Omega\text{m}$ deduced from SCI inversion of FHEM data as shown in Fig. 33. Black dots represent exposed bedrock locations. Thin black, thicker black and green lines represent FHEM, 2D resistivity and seismic refraction lines, respectively. Coloured circles show bedrock depth confirmed by drilling. White areas in centre of the map represent depth to bedrock deeper than 30 m. 46

Figure 37: Depth of a resistivity zone $> 200 \Omega\text{m}$ deduced from SCI inversion of FHEM data as shown in Fig. 33. Black dots represent exposed bedrock locations. Thin black, thicker black and green lines represent FHEM, 2D resistivity and seismic refraction lines, respectively. Coloured circles show bedrock depth confirmed by drilling. White areas in centre of the map represent depth to bedrock deeper than 30 m. 47

Figure 38: Depth of a resistivity zone $> 500 \Omega\text{m}$ deduced from SCI inversion of FHEM data as shown in Fig. 33. Black dots represent exposed bedrock locations. Thin black, thicker black and green lines represent FHEM, 2D resistivity and seismic refraction lines, respectively. Coloured circles show bedrock depth confirmed by drilling. White areas in centre of the map represent depth to bedrock deeper than 30 m. 48

Figure 39: Modified plot of depth restricted to approx. 25 m and use of fewer colors for resistivity zone $> 200 \Omega\text{m}$ as shown in Fig. 37. 200 Ωm was assumed as an indication of bedrock resistivity. Black dots represent exposed bedrock locations. Thin black, thicker black and green lines represent FHEM, 2D resistivity and seismic refraction lines, respectively. Coloured circles show bedrock depth confirmed by drilling. White areas in centre of the map represent depth to bedrock deeper than 30 m. 49

Figure 40: Comparison of FHEM, RCPTu and clay type interpretation near geotechnical drilling point 11 (see table 4 and Fig. 1). Vertical and horizontal dashed lines are unleached-leached clay boundary (10 Ωm) and FHEM DOI, respectively. 51

Figure 41: Comparison of FHEM, RCPTu and clay type interpretation near geotechnical drilling point 2 (see table 4 and Fig. 1). Vertical and horizontal dashed lines are unleached-leached clay boundary (10 Ωm) and FHEM DOI, respectively. 52

Figure 42: Comparison of FHEM, 2D Resistivity survey and clay type interpretation near geotechnical drilling point A (see table 4 and Fig. 1). Vertical and horizontal dashed lines are unleached-leached clay boundary (10 Ωm) and FHEM DOI, respectively. 53

Figure 43: Comparison of FHEM, 2D Resistivity survey and clay type interpretation near geotechnical drilling point 202 (see table 4 and Fig. 1). Vertical and horizontal dashed lines are unleached-leached clay boundary (10 Ωm) and FHEM DOI, respectively. 53

TABLES

Table 1: Instrument Specifications.....13

Table 2: Frequencies and coil configurations of Hummingbird electromagnetic system.....14

Table 3: Skin depth values for FHEM frequencies and typical resistivity values.....19

Table 4: Location of RCPTu and geotechnical drills and their distance from FHEM and 2D resistivity measurements.....48

1. INTRODUCTION

On January 1st 2012, there was a landslide at Byneset, Trondheim due to remolding of quick clay (Solberg et al. 2012a). The landslide area is surrounded mostly by agricultural lands. The geology in the area consists of old ocean floor with outcropping bedrock at several places. The area has a lot of ravines and traces of landslide activity (Solberg et al. 2015). Prehistorically, the sea level was ~ 160 m higher than the present sea level (Reite et al. 1999). The sediments in the area mainly consist of marine clay. Subsequent leaching by fresh groundwater alters the chemical composition of the pore water in the marine clay, and “quick clay” may develop. The quick clay completely liquefies when remolded and it may result in large landslides.

2D resistivity survey is useful to delineate ground water and marine clay deposits (e.g. Solberg et al. 2012b, Kalscheuer et al. 2013, Sauvin et al. 2014). Salt-holding or unleached clay shows a resistivity less than 10 Ωm (Solberg et al. 2011). Washing out the salt and its replacement with fresh water, results in leached clay with higher resistivity that may range between 10 Ωm - 100 Ωm . The leached clay may or may not contain quick clay. Presence of the quick clay can be confirmed with geotechnical drilling and testing of soil samples. Therefore, various geophysical surveys including 2D resistivity, Frequency-domain Helicopter-borne ElectroMagnetic (FHEM), Seismic refraction survey were performed in the area to investigate marine sediment, possible quick-clay, and other deposits.

2D resistivity survey with electrode spacing 10 m provides a detailed subsurface resistivity down to about hundred meters of depth which can help in differentiating between areas containing leached and unleached clay. However, it needs lots of manpower and it is relatively time-consuming. FHEM survey may also provide high resolution subsurface resistivity though not as detailed as 2D resistivity survey, but it can cover a larger area in a rather short time. Our FHEM equipment is an old Hummingbird system (Geotech, 1997) and specially designed for mineral prospecting but it may still provide useful information about marine clay deposits. Modern designed FHEM system such as RESOLVE by Fugro (Abraham et al., 2012; Fugro, 2010) has more no. of frequencies and operates at higher frequencies which could be more appropriate for ground water and such environmental studies. SKYTEM, VTEM are other helicopter-borne EM systems which do measurements in the time domain and sometime better suited for groundwater and clay layer mapping studies (Allard, 2007; Siemon et al., 2009; Ley-Cooper and Munday, 2013).

Resistivity piezoCone Penetration Test (RCPTu) measurements provide direct and in-situ measurement of the subsurface resistivity and other physical properties. Resistivity obtained by RCPTu can also be used to cross-check and validate the resistivity values obtained from the methods such as 2D resistivity and FHEM survey. Seismic refraction survey can provide us information about various seismic velocity layers and bedrock depth.

To extract useful information and interpret FHEM data accurately, it is important to collect stable, less noisy data and calibrate the system properly. In starting of each survey year, we calibrate and test our survey equipments. We calibrated and set the correct phasing to the system with help of a standard ferrite bar. A proper gain to FHEM system was set using a standard reference coil (Geotech, 1997). Recent literature suggests even a more accurate calibration technique with the help of other measurements e.g. borehole resistivity data, 2D resistivity survey, flying over sea-water and flying at various altitude at same locations to calculate correct subsurface resistivity (Minsley et al., 2012 and 2014; Ley-Cooper et al., 2006 and 2007; Deszcz-Pan et al., 1998). We planned FHEM survey in Byneset to investigate

its ability in mapping of clay layers. Two 1D inversion codes from University of British Columbia (UBC) and University of Aarhus are tested and used to invert the FHEM data. Results from FHEM survey are verified with results from 2D resistivity, seismic refraction surveys, exposed bedrock locations and RCPTu. Depth of the bedrock is also available at few locations from earlier drillings in the area.

2. LOCATON AND SURVEY SPECIFICATION

The survey area is located in Byneset, Sør-Trøndelag County, Norway. Figure 1 shows the survey area in UTM zone 32N coordinate with profile lines of various geophysical surveys. The FHEM survey was carried out in June 2013, in E-W direction, shown as black lines. Line spacing for the survey was 100 m in northern part and 200 m in the southern part of the area. The line directions were selected according to the geological strike in the area in E-W direction. The helicopter survey covered total 218 line km in an area of 30 km², with average bird height of 59 m and average speed of 97 km/h. Profiles of 2D resistivity and seismic refraction surveys were performed in October and November 2013. They are shown by red and blue lines, respectively. The landslide of 1st January 2012 occurred at the western end of refraction seismic profile along line 142 and it is shown by a black cross symbol. Green dots in the figure represent earlier geotechnical drilling locations performed by Trondheim municipality and other companies. Results of the geotechnical investigations are not discussed here but a detailed comparison of 2D resistivity, refraction seismic and geotechnical results can be found in Solberg et al. (2015).

2.1 Location of geotechnical drilling and bedrock sampling

In general, presence of quick clay may be probed through geotechnical sounding by low and decreasing drilling resistance. However, differentiating between leached clay, quick clay, and occasionally other deposits, may be difficult. For this problem, testing of samples in laboratory is the most reliable method, but also subsurface resistivity measurements like 2D resistivity survey (e.g. Solberg et al. 2012b) and RCPTu can help in the interpretation of drilling profiles.

Some of the clay samples collected from possible quick clay and other locations (not shown in this report but detailed by Solberg et al., 2015) were examined for salt content to confirm it as quick clay. Two locations (A and 202) are shown by black diamond where we compare results of FHEM and 2D Resistivity survey as 1D plots with interpretation of clay types from geotechnical drilling and 2D resistivity survey. Two more locations are shown as black diamond (2 and 11) where downhole resistivity was measured using the RCPTu method. Black dots show some exposed bedrock locations mapped by NGU. There were also four locations where bedrock depth was confirmed by drilling and they are discussed later in this report when we discuss about bedrock depth map derived from FHEM data.

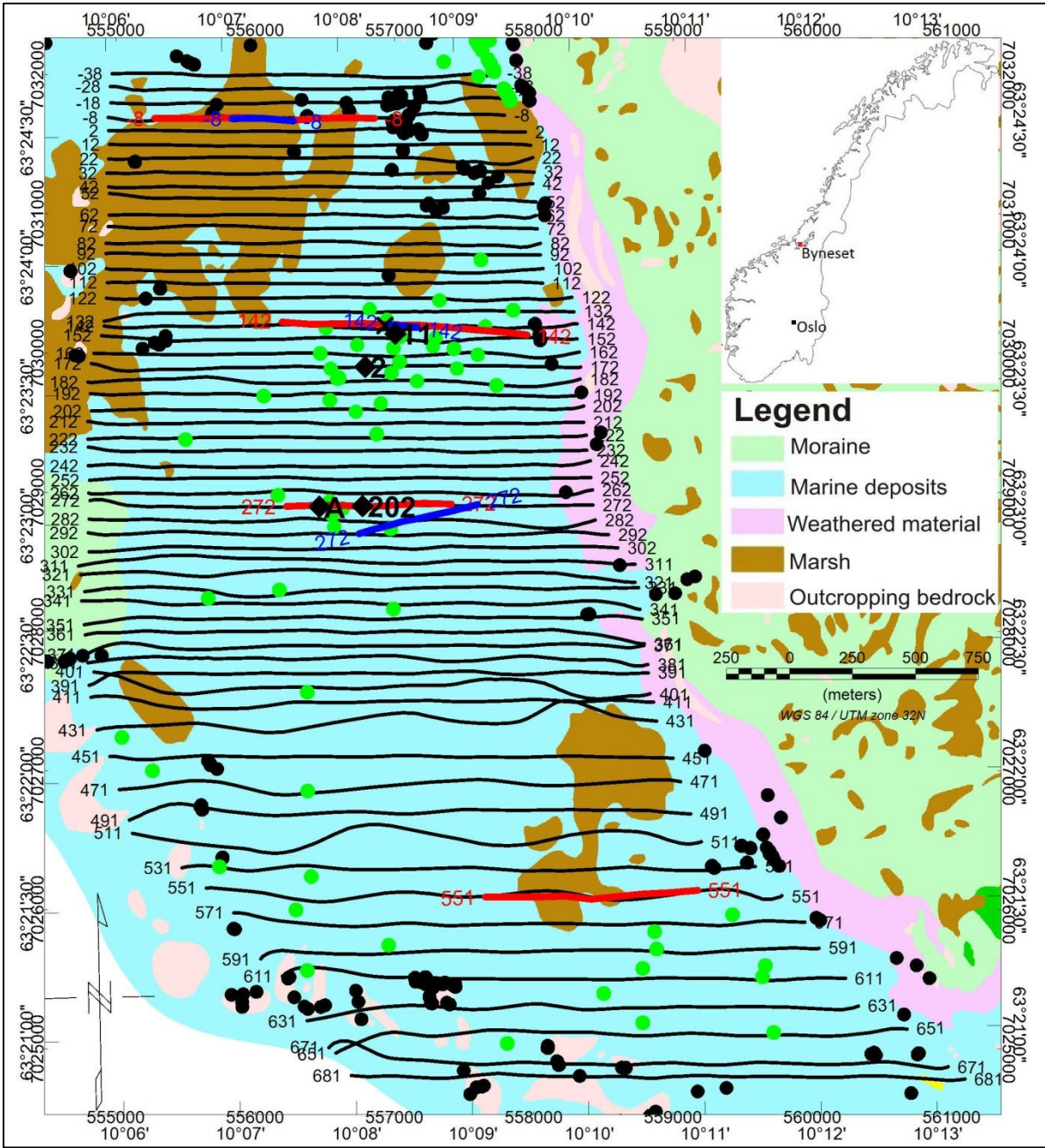


Figure 1: Quaternary geological map of the survey area and profiles of the geophysical surveys. See text for details.

2.2 Ground geophysical survey parameters

Four 2D resistivity profiles and three refraction seismic profiles were carried out along four of the helicopter survey lines in the autumn of 2013.

2.2.1 2D Resistivity survey

2D resistivity data was acquired with the Lund system at 10 m electrode spacing using an ABEM Terrameter LS in multi gradient-array configuration (Dahlin, 1993) along part of the lines L-8, L142, L272 and L551 (Fig. 1). Details of the measurements are given in Solberg et al. (2015).

Figure 2 shows the classification of sediments using resistivity values interpreted from 2D resistivity surveys by NGU in different projects in areas with marine deposits (e.g. Solberg et al. 2008, 2011, 2012a and 2012b). Same classification of sediments is used in this study for resistivity interpreted from 2D resistivity and FHEM data. It is important to notice that local variations in different areas may influence the data and the interpretation.

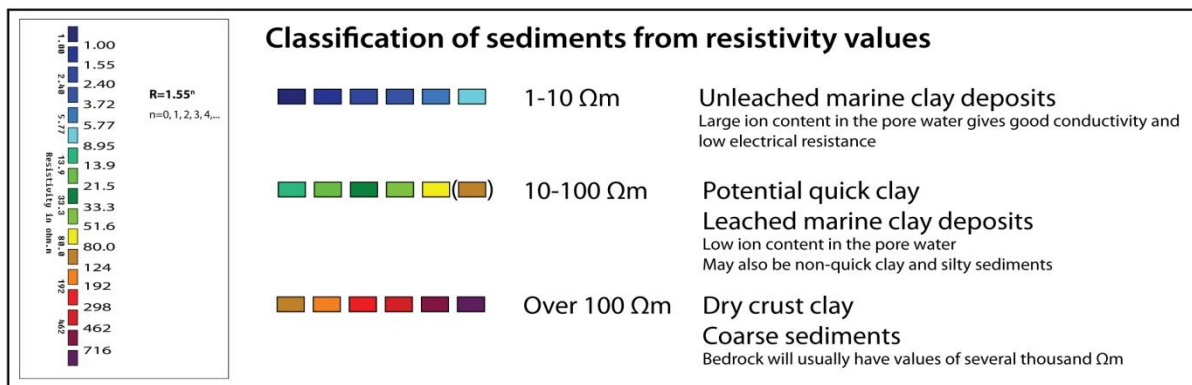


Figure 2: Classification of sediments based on resistivity values obtained from interpretation of 2D resistivity measurements in different projects (from Solberg et al. 2008).

2.2.2 Refraction seismic survey

Refraction seismic survey was performed along parts of three of the 2D resistivity profiles to estimate depth of the bedrock. The data acquisition was made using a seismic recording system ABEM TERRALOC MK6 with 24 channels. Geophone spacing was 10 m (short cable) and 20 m (long cable) and shooting point distance was 110 m. Five to nine shots were fired for each 24 geophone spread. Some of them were also fired outside the spread to get refractions from the bedrock. Energy source for the shootings was ordinary dynamite with electrical ignition. The explosive charge was placed in the ground in a hole made with a crowbar. For each shot, approx. 100 grams of dynamite were used.

2.3 Airborne Survey Parameters

NGU used a Hummingbird™ EM and magnetic helicopter survey system (Fig. 3) designed to obtain low altitude and detailed airborne magnetic and EM data (Geotech 1997). In addition, a 1024 channel Radiation Solutions RSX-5 gamma-ray spectrometer was placed on the helicopter to map ground concentrations of equivalent uranium (eU), equivalent thorium (eTh) and potassium (K). We collected airborne EM, magnetic, and radiometry data from the area but only EM data is of our primary interest in mapping of the clay layers. Therefore, magnetic and radiometric data are not interpreted and presented in this report.

A 7.5 m long bird housing magnetic and EM sensors was towed at 30 m below the helicopter giving an average sensor height of 59 m above the topographic surface. A Eurocopter AS350-B3 operated by Heliscan As was used for the survey. Gamma-rays spectrometer was installed under the belly of the helicopter to register natural gamma ray radiation simultaneously with the acquisition of magnetic and EM data.

The ground speed of the aircraft varied from 50 to 137 km/h depending on the topography, wind direction and wind speed. On average the ground speed during measurements was calculated to 98 km/h. The study area in Byneset, Trondheim is not mountainous but due to safety, the pilot could perform the survey at an average bird height of 60 m only which might have reduced efficacy of the collected data. Magnetic data were recorded at 0.2 second intervals resulting in approximately 6 m spacing. EM data were recorded at 0.1 second intervals resulting in data with an average sample increment of 3 m. Spectrometry data were recorded every 1 second giving a data spacing of approximately 30 meter. The above parameters were designed to allow for sufficient details in the data to detect subtle anomalies that might represent mineralization and/or rocks of different lithological and petrophysical composition.

Navigation system used GPS/GLONASS satellite tracking systems to provide real-time WGS-84 coordinate locations for every second. The accuracy achieved without differential corrections was reported to be less than ± 5 m in the horizontal directions. The GPS receiver antenna was mounted externally to the tail tip of the helicopter. Altitude of the flight was determined using radar altimeter installed in front of the helicopter.

2.3.1 Airborne Survey Instrumentation

The airborne instrument specifications are given in table 1. Frequencies and coil configuration for the Hummingbird EM system are given in table 2.

Table 3: Instrument Specifications

Instrument	Producer/Model	Resolution/Accuracy	Sampling frequency
Magnetometer	Scintrex Cs-2	0.002 nT/2.5 nT	5 Hz
Base magnetometer	Scintrex EnviMag	0.1 nT	0.33 Hz
Electromagnetic	Geotech Hummingbird	1 – 2 ppm	10 Hz
Gamma-ray spectrometer	Radiation Solutions RSX-5	1024 channels, 16 liters down, 4 liters up	1 Hz
Radar altimeter	Bendix/King KRA 405B	± 3 % for 0 – 500 feet ± 5 % for 500 – 2500 feet	1 Hz
Pressure/temperature	Honeywell PPT	± 0.03 % FS	1 Hz
Navigation	Topcon GPS-receiver	± 5 meter	1 Hz
Acquisition system	Geotech Ltd and NGU In-house software		

Table 4: Frequencies and coil configurations of Hummingbird electromagnetic system.

Coils:	Frequency	Orientation	Separation
A	7701 Hz	Coaxial	6.2 m
B	6606 Hz	Coplanar	6.2 m
C	980 Hz	Coaxial	6.0 m
D	880 Hz	Coplanar	6.0 m
E	34133 Hz	Coplanar	4.9 m

The EM, magnetic, radiometric, altitude and navigation data were monitored on the operator's display during the flight for quality control and survey progress. Later, on same or next day it was viewed at NGU for detailed quality control.

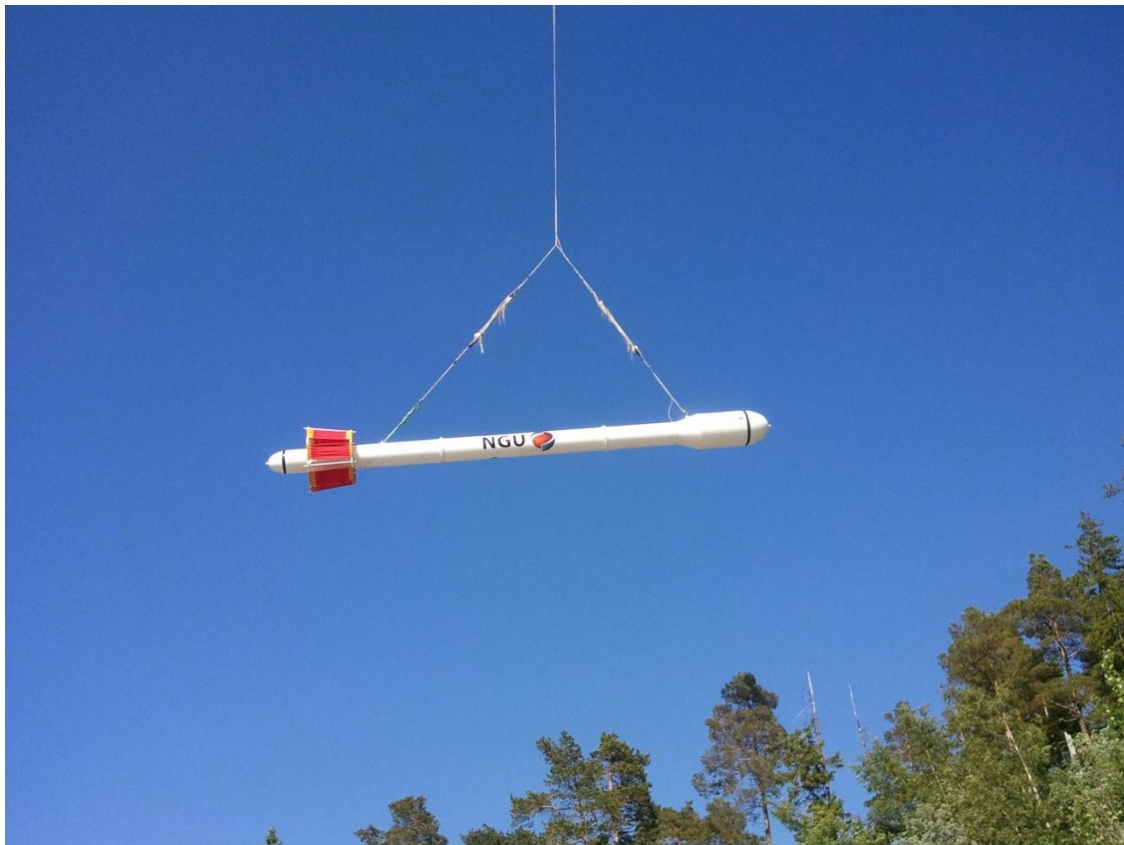


Figure 3: Hummingbird system in the air during a survey.

2.3.2 Calibration

The FHEM system was calibrated for phasing with the help of a ferrite bar and for gain to correct amplitude of in-phase (real part) and quadrature (imaginary part) measurements using calibration coils as recommended by manufacturers (Geotech, 1997). A short flight was also made over seawater of the Trondheimsfjord near the survey area to cross-check seawater resistivity value from FHEM data. After processing and 1D inversion, seawater resistivity was interpreted to be approx. $0.25 \Omega\text{m}$ which is very close to the true value.

3. DATA PROCESSING AND RESULTS

All the survey data were processed and interpreted at NGU office in Trondheim. Airborne EM, magnetic and radiometric data were collected, however only airborne EM data is processed, interpreted and presented in this report.

3.1 Ground geophysical surveys

2D resistivity and refraction seismic ground surveys were performed as a follow-up of airborne EM survey. The surveys were carried out along parts of four EM lines (L-8, L142, L272 and L551, Fig. 1). Refraction seismic survey was not performed along line L551 due to unsuitable field condition. A visual inspection of the area was also done to map location of exposed and shallow bedrock. They are plotted as black dots in Fig. 1.

3.1.1 Refraction seismic survey

Refraction seismic data were interpreted manually using crossover distance, intercept time and Hagedoorns +/- method (Reynolds, 2011). Results from three profile lines are shown in the Figs. 4 to 6. Legend of seismic interpretation is shown in Fig. 4a. Figure 4b shows seismic profile interpretation along line -8. It shows three velocity layers, firstly a shallow layer, close to the ground of approx. 500 m/s velocity. This can be interpreted as an unconsolidated layer of clay and partly bog/peat. The second layer has a seismic velocity of approx. 1500 m/s and consists of water-saturated deposits, probably dominated by marine clay. The deepest layer is bedrock with seismic velocity approx. 3200-6500 m/s starting from the ground level at east end, deepest in the middle approx. 50 m above mean sea level (m.s.l.) and narrowed at the west end. The low bedrock velocity values can be caused by zones of either intensive fracturing/crushing of bedrock or deep weathering in the bedrock. In addition, seismic velocity variation in bedrock can partly be caused by variations in bedrock type. Seismic profiles along line 142 and line 272 also show similar layers but the sediment thickness is quite different. Along line L142 (Fig. 5), the sediment thickness varies between 8 to 18 m and the bedrock is approx. 76-88 m above m.s.l. Along line L272 (Fig. 6), the sediment thickness is approx. 120 m and the bedrock is about 40 m below m.s.l.

(a)

Legend	
————	Terrain surface, Superficial deposits (Unsaturated sand/clay and bog/peat)
————	Layer 2, Superficial deposits (Water saturated material, mostly clay dominated)
- - -	Layer 2, (Only along line L272 outside the geophone spread)
————	Layer 3, Bedrock
- - -	Layer 3, Bedrock (Only along line L272 outside the geophone spread)
↓	Shot point
1500	Seismic velocity (m/s)

Figure 4: (a) Legend used in refraction seismic interpretation.

(b)

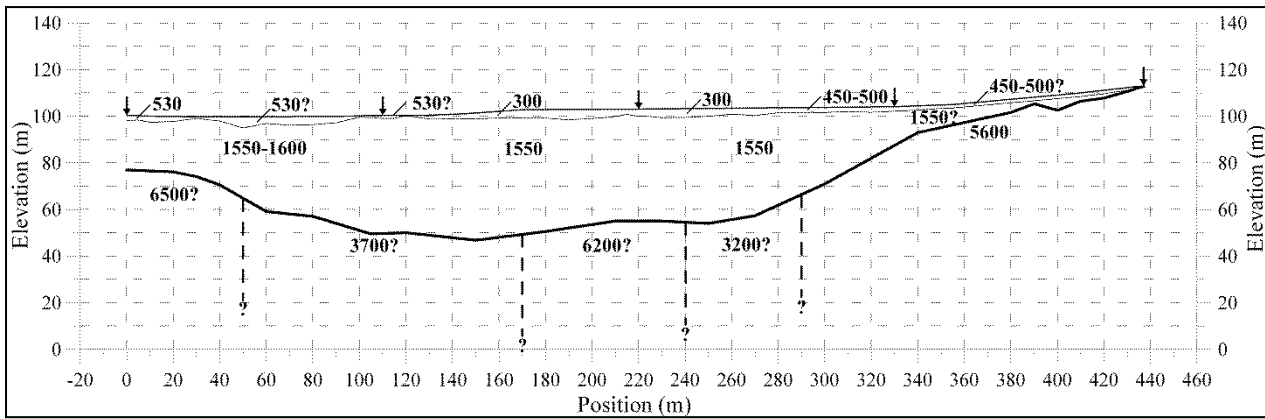


Figure 4: (b) Refraction seismic interpretation along line -8.

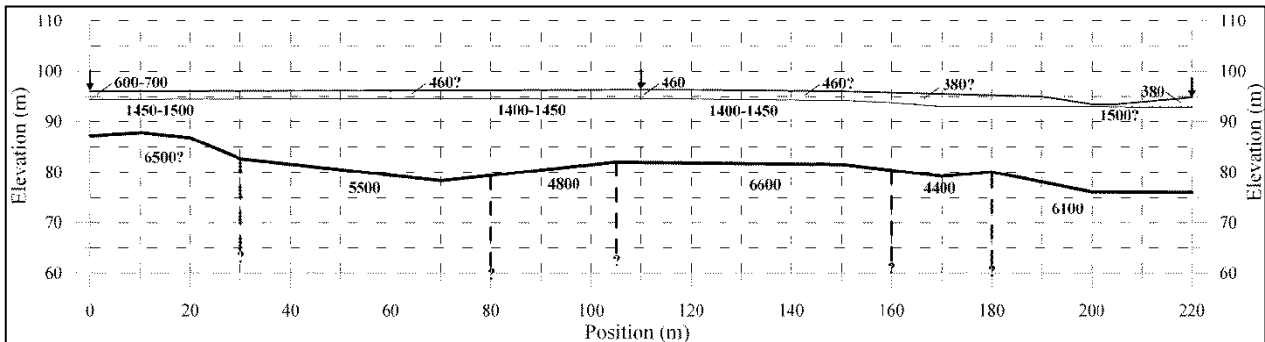


Figure 5: Refraction seismic interpretation along line 142.

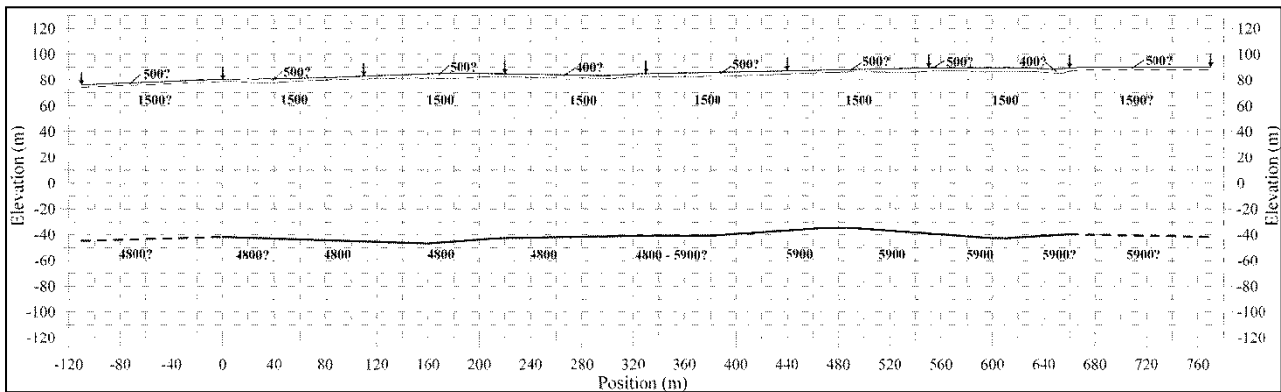


Figure 6: Refraction seismic interpretation along line 272.

3.1.2 2D Resistivity survey

2D resistivity data was inverted using RES2DINV code from Geotomo software (Loke, 2010). We used standard inversion of L2 norm and V/H filter as 0.5. Results from the four lines are shown in Figs. 7 to 10. Data fitting was not very good due to complex structures. We observed RMS error of 16 to 28 which should be lower between 1 to 10 % for a good data fitting. The plots are generated in Matlab to have same color scale as for resistivity from FHEM plots. This color scale is slightly different in color representation in comparison to NGU's standard color presentation of 2D resistivity data (Fig. 2). Two velocity layer boundaries interpreted from refraction seismic data along parts of the lines are shown (dashed

black lines) together with its topography line (dashed red line). The topography from seismic survey along Line 272 (Fig. 9) does not match well with topography of the 2D resistivity survey because this seismic survey line was performed southward due to the field constraints (Fig. 1). In general, blue areas show unleached marine clay and green areas show leached/possible quick clay areas from resistivity interpretation.

Figure 7 presents resistivity cross-section along line -8. There is a good agreement between the 2D resistivity and seismic interpretations for bedrock boundary. It is interpreted at approx. 50 m above m.s.l. from seismic refraction data and also by 2D resistivity data. 2D resistivity interpretation along line 142 depicts a resistivity layer of 50 to 100 Ωm at approx. 70 m above m.s.l. with discontinuities at approx. 700, 850 and 1300 m along line 142 (Fig. 8) which matches with bedrock layer boundary interpreted by refraction seismic data. However, refraction seismic interprets bedrock layer continuous at 850 m. Figure 9 depicts bedrock layer along line 272 at approx. 40 m below m.s.l. by seismic refraction data which corresponds to approx. 20 Ωm layer with a discontinuity at 700 m from 2D resistivity interpretation. The unleached marine clay above this layer and below a very shallow and thin possible quick clay layer is interpreted of approx. 60 m thickness. Resistivity profile along line 551 (Fig. 10) shows a continuous low resistive layer of approx. 50 Ωm at 70 m above m.s.l. interpreted as possible quick clay and then a thick unleached marine clay of approx. 50 m thickness and at approx. 50 m below m.s.l. More detailed interpretation of resistivity profiles with comparison to geotechnical drilling data is presented in Solberg et al. (2015).

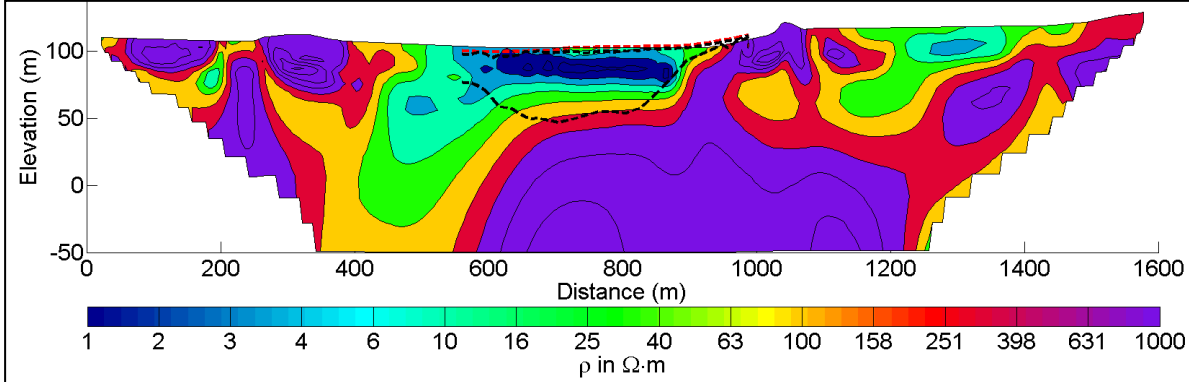


Figure 7: Inverted model from 2D resistivity data along line -8. Dashed black lines show seismic velocity boundaries and dashed red line shows topography of seismic profile. Lower dashed black line represents interpreted bedrock depth.

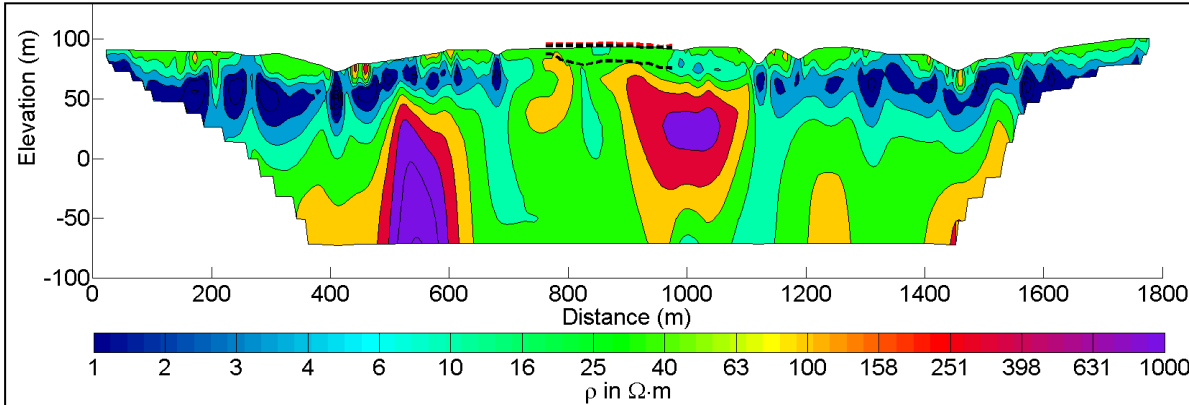


Figure 8: Inverted model from 2D resistivity data along line 142. Dashed black lines show seismic velocity layers and dashed red line shows topography of seismic profile. Lower dashed black line represents interpreted bedrock depth.

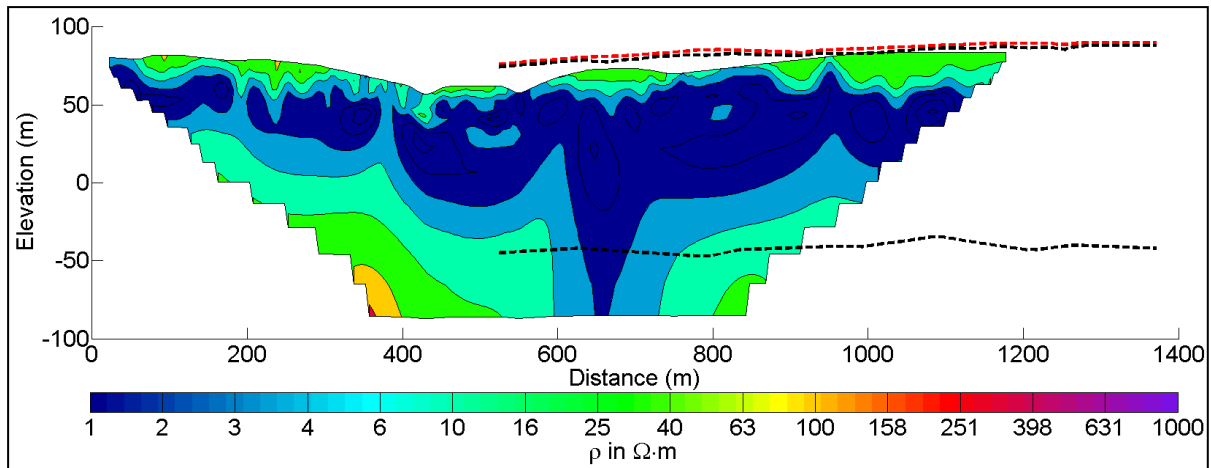


Figure 9: Inverted model from 2D resistivity data along line 272. Dashed black lines show seismic velocity layers and dashed red line shows topography of seismic profile. Lower dashed black line represents interpreted bedrock depth.

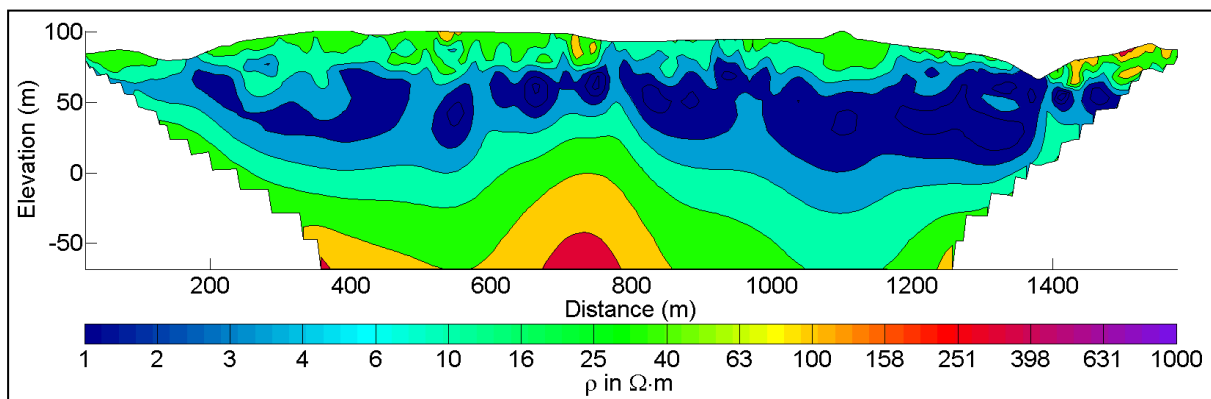


Figure 10: Inverted model from 2D resistivity data along line 551. There was no seismic line along this profile.

3.2 Processing of FHEM Data

The in-phase and quadrature values for each of the five coil sets (for each frequency) of the electromagnetic system were recorded. In-phase and quadrature data were filtered with 3 fiducials non-linear filter to eliminate spherical spikes which were identified as irregular spikes of large amplitude in the records. Simultaneously, the 20 fiducials low-pass filter was also applied to suppress high frequency components of instrumental and cultural noise.

In order to remove the effects of instrument drift caused by gradual temperature variations in the transmitting and receiving circuits, background responses were recorded during each flight. To obtain a background level, the bird was raised to an altitude of approximately 1200 ft above the topographic surface so that no electromagnetic responses from the ground were present in the measurements. The EM traces observed at this altitude correspond to a background (zero) level of the system. If these background levels were recorded at 20-30 minute intervals, then the drift of the system (assumed to be linear) could be removed from the data by resetting these points to the initial zero level of the system (Valleau, 2000). This drift was removed on a flight-by-flight basis before any further processing was carried out. Geosoft HEM module was used for applying drift correction. Later, residual instrumental drift, often non-linear, were manually removed after splitting the data in lines on line-to-line basis.

After leveling of the HEM data, apparent resistivity was calculated from in-phase and quadrature data using a homogeneous halfspace model of the Earth (Whitehead, 2005) for five frequencies separately. Threshold of 3 ppm was set for inversion of three higher frequencies of 6606, 7001 and 34133 kHz and 2 ppm for lower frequencies of 880 and 980 Hz. Higher frequencies provides resistivity information from shallower depth and lower frequency provides resistivity information from greater depth. Approximate penetration depth of EM signal is assumed around one skin depth d and it can be calculated using skin depth formula knowing EM signal frequency f and resistivity ρ as follows

$$d = 503 \sqrt{\rho/f} \quad (1)$$

Table 3: Skin depth values for FHEM frequencies and typical resistivity values.

Skin depth (m)						
Frequency (Hz)		880	980	6606	7001	34133
Resistivity (Ωm)	10	54	51	20	19	9
	100	170	161	62	60	27
	1000	536	508	196	190	86

Table 3 presents skin depth values for FHEM frequencies and typical resistivity values important to this study. We can see it gets as low as 9 m for highest frequency 34133 Hz and low resistivity 10 Ωm . In case of bedrock (1000 Ωm or more), skin depth is around 536 m for lowest frequency 880 Hz. Secondary electromagnetic field decays rapidly with the distance z (height of the sensors from the target) as $1/z^2$ to $1/z^5$ depending on the shape of the conductors and, at certain height, signals from the ground sources become comparable with instrumental noise.

Leveling errors or precision of leveling can sometimes lead to appearance of artificial resistivity anomalies when data were collected at high instrumental altitude. Application of a threshold height allows excluding such data from an apparent resistivity calculation, though not completely. It is particularly noticeable in low frequencies datasets. Therefore, resistivity data were visually inspected for artificial anomalies associated with high altitude measurements. Finally, revised resistivity data were gridded with a cell size of 30 m. Gridded apparent resistivity data from five frequencies of FHEM data are presented in Figs. 11 to 15. Apparent resistivity of several thousand Ωm (pink color) can be interpreted as outcropping bedrock. All the frequencies suggest presence of bedrock at various places which means it is exposed at surface and extending deeper. Middle and southern sides of the survey area are shown less to moderate resistive (light blue to green and yellow color) by higher frequencies 34 kHz, 7 kHz and 6.6 kHz. It is further less resistive (dark blue color) as shown by 980 and 880 Hz data. This indicates that these areas could contain silty sand and quick clay at surface. However, it is unleached marine clay at the depth.

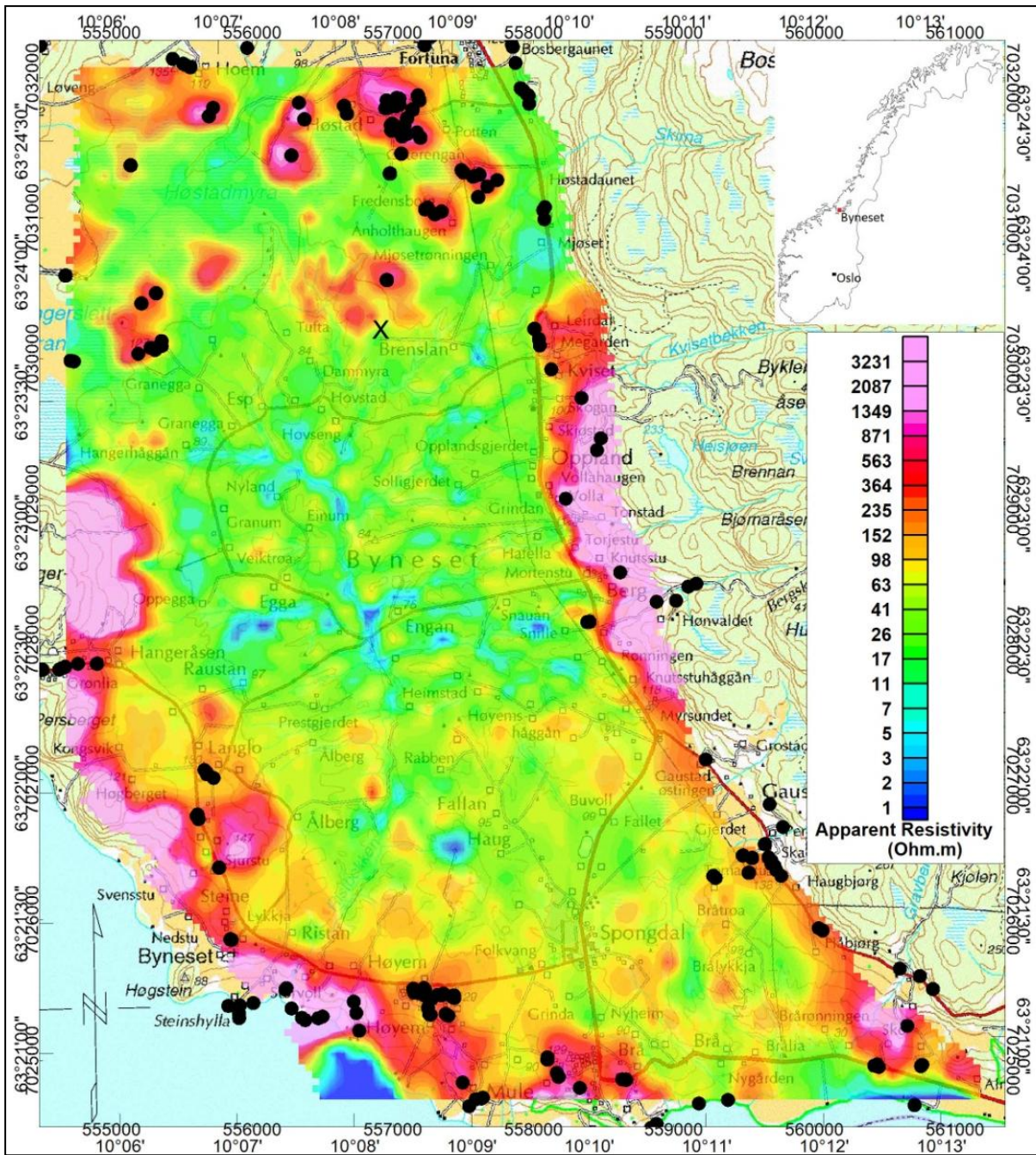


Figure 11: Homogeneous half-space inversion of FHEM data at frequency 34 kHz coplanar coils. Exposed bedrock locations are marked by black dots.

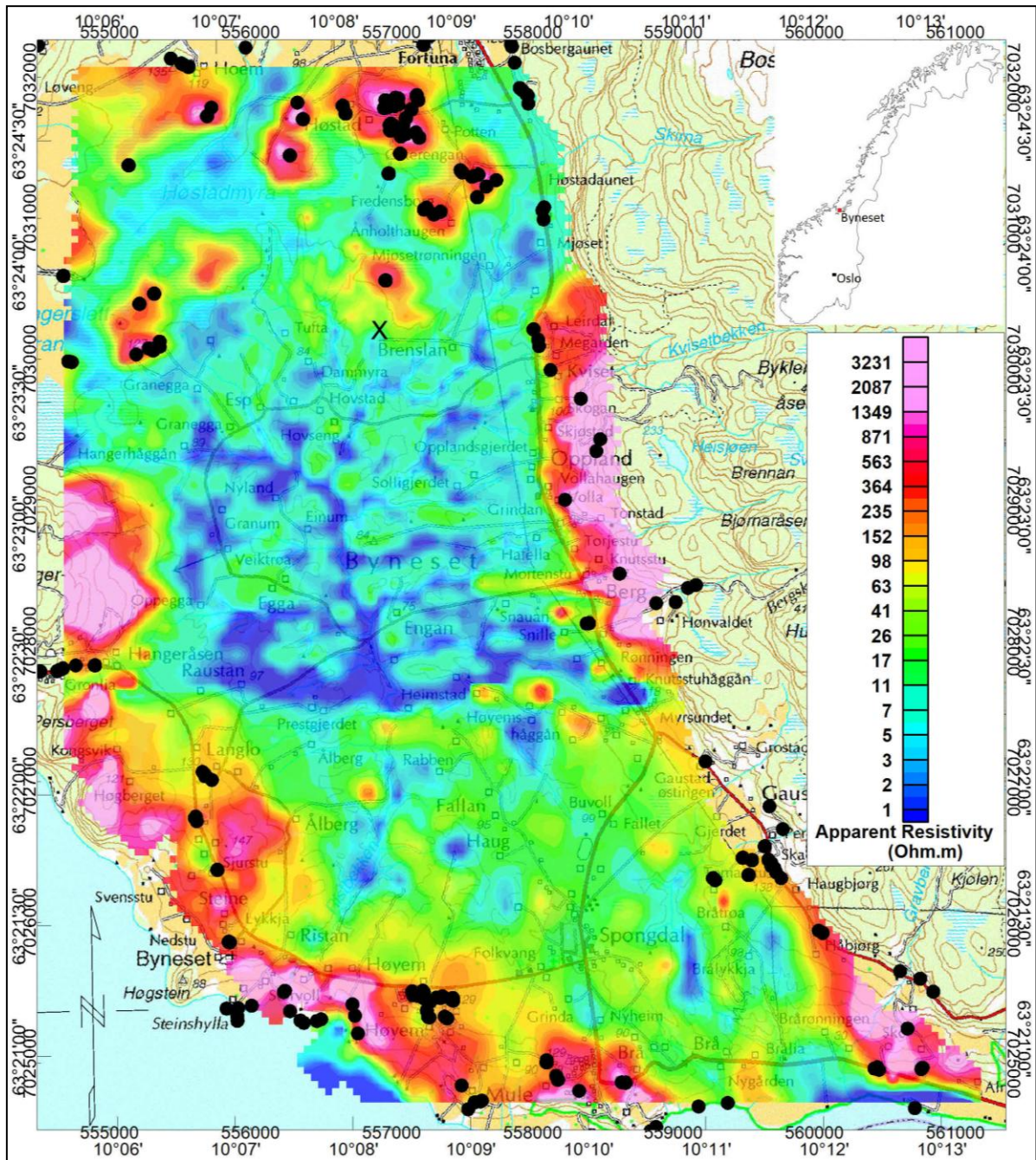


Figure 12: Homogeneous half-space inversion of FHEM data at frequency 7 kHz coaxial coils. Exposed bedrock locations are marked by black dots.

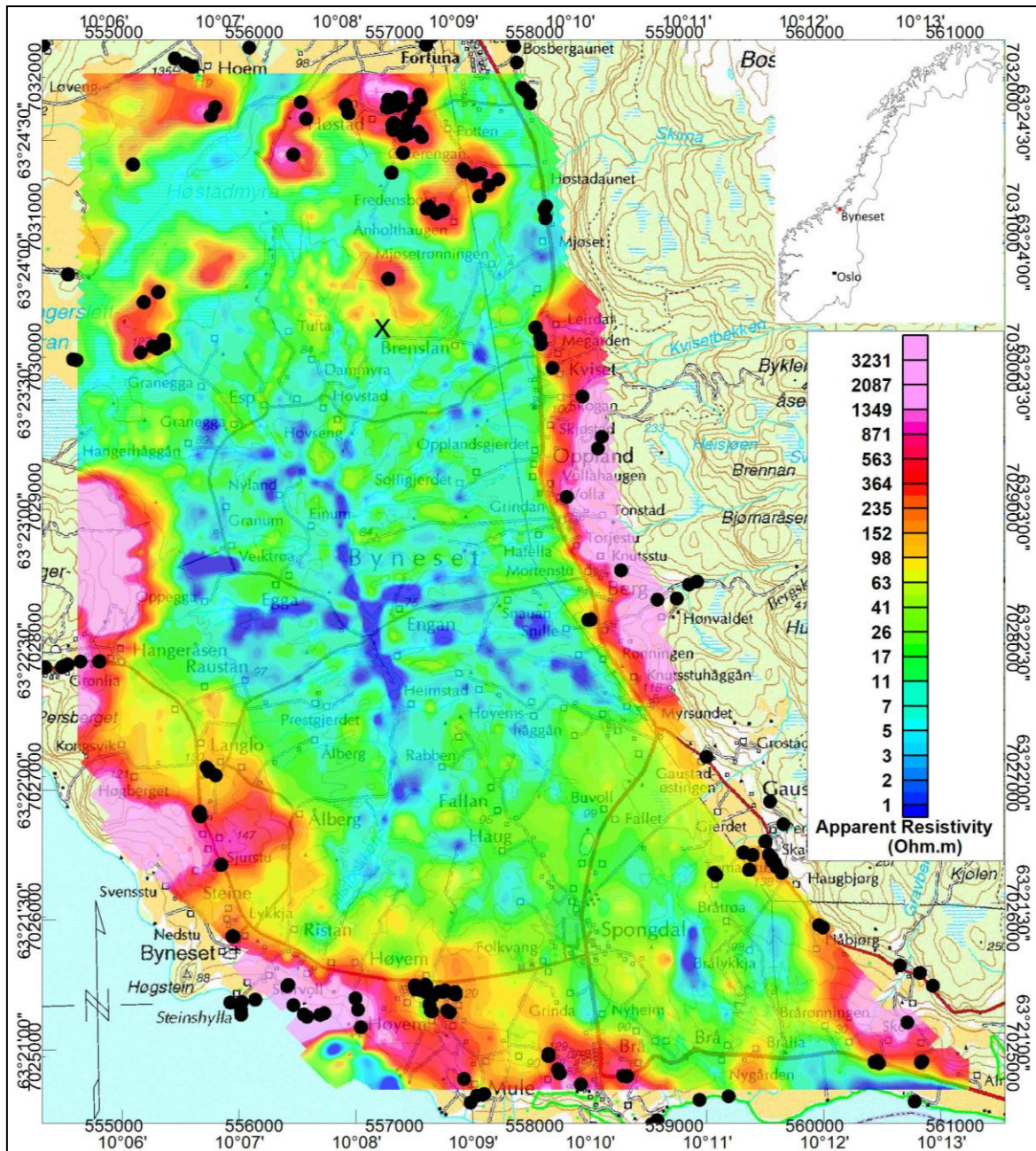


Figure 13: Homogeneous half-space inversion of FHEM data at frequency 6.6 kHz coplanar coils. Exposed bedrock locations are marked by black dots.

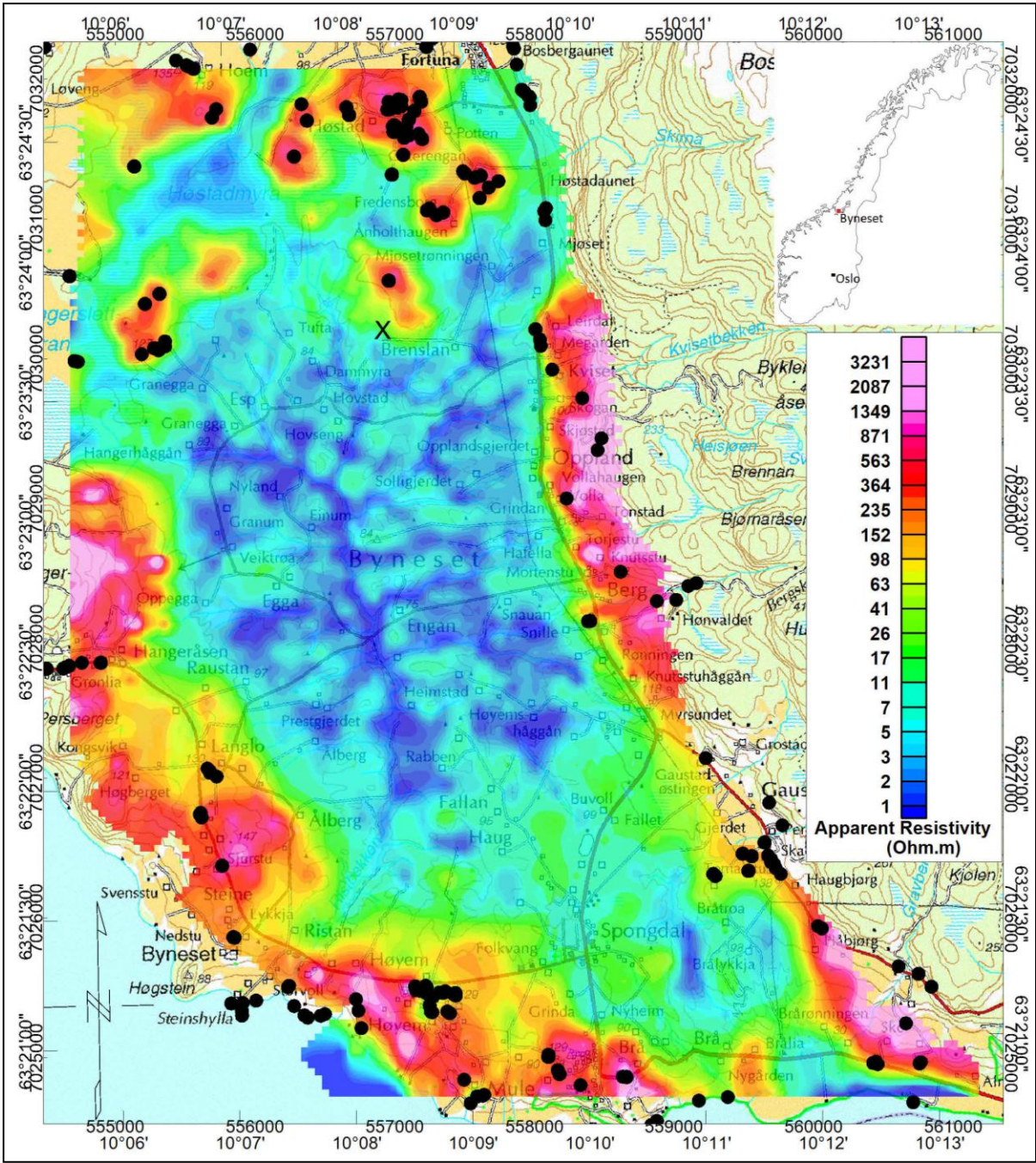


Figure 14: Homogeneous half-space inversion of FHEM data at frequency 980 Hz coaxial coils. Exposed bedrock locations are marked by black dots.

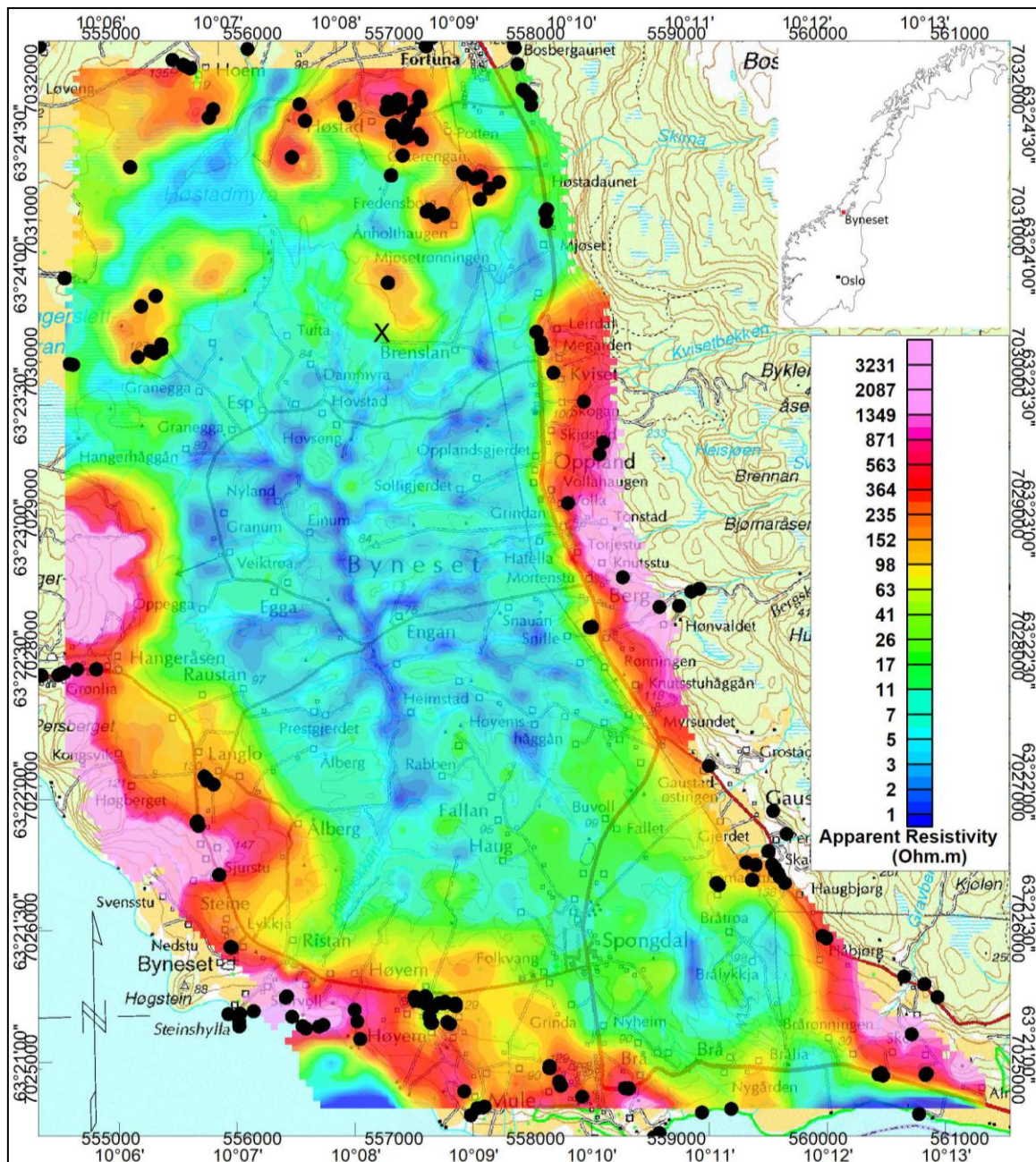


Figure 15: Homogeneous half-space inversion of FHEM data at frequency 880 Hz coplanar coils. Exposed bedrock locations are marked by black dots.

3.3 1D Inversion of FHEM data

To decipher true resistivity from FHEM data, two 1D (one-dimensional) inversion codes EM1DFM from University of British Columbia (EM1DFM manual, UBC 2000) and AarhusInv from Hydro Geophysics Group, Aarhus University (AarhusInv manual, 2013), are tested to invert helicopter EM data. Processed FHEM data were averaged using a running average of 10 points to produce data at approx. 30 m interval along flight lines to prepare it for inversion. Resistivity values obtained from inversion still could not be an accurate representation of the subsurface because 1) inversion codes are simple isotropic 1D inversions and real earth is 3D (three dimensional) and anisotropic, 2) inversion of secondary magnetic field data alone (without electric field data) provides ambiguous resistive models specially for hard rock areas where measured response of EM signal is very low. A brief description about both codes and comparison of the results from these codes is presented in this section.

3.3.1 UBC's 1D code: EM1DFM

EM1DFM stands for electromagnetic (EM) one-dimensional models (1D) frequency-domain (F) magnetic dipole transmitters and receivers (M). This inversion program is designed to construct 1D conductivity/resistivity models, using any type of frequency domain loop-loop geophysical EM data. The inversion program can construct an electrical conductivity model as well as a magnetic susceptibility model. Models of the Earth are composed of many layers of uniform conductivity/susceptibility with fixed interface depths. The value of the conductivity/susceptibility in each layer is sought by the inversion. Multiple soundings can be handled in a single run of the program. Each sounding is interpreted independently with a one-dimensional model produced under the sounding location. When all soundings have been inverted, a composite two-dimensional model is written out to facilitate interpretation of a line of soundings. Details of the inversion method can be found in Farquharson et al. (2003) and inversion manual (EM1DFM manual, UBC 2000).

Inversion of FHEM data (In-phase and quadrature) using EM1DFM code was performed by Alexei Rodionov (AR Geoconsulting Ltd, Canada) starting with a 100 Ω m half-space and assuming 10 % standard noise in the data. Inverted resistivity model is plotted in Matlab to match the color scale of the resistivity models obtained by the two codes EM1DFM and AarhusInv and also from 2D resistivity survey. Figures 16 to 23 show inverted resistivity models and fitting between field (measured) data and computed data from the model. Seismic velocity boundaries obtained from refraction seismic survey are also plotted by thick dashed black lines on the resistivity model. Topography of seismic profile line is shown by dashed red line. Length of the 2D resistivity survey along these FHEM lines are also plotted by a thinner dashed line.

Inverted model from FHEM data along line -8 (Fig. 16) matches broadly with both 2D resistivity and seismic interpretations. We see three conductive zones at 1000 m, 1700 m and 2600 m. Conductive zone at 1000 m is extending to 70 m above m.s.l., but the 2D resistivity and seismic data suggested that it goes deeper. Both the conductive zones shown by 2D resistivity data are also shown by FHEM data. There is also a very thin and shallow conductive zone shown at 400 m in FHEM data which is not present in the model from 2D resistivity data. There is good fitting between measured and computed data for all frequencies except for 34 kHz (Fig. 17).

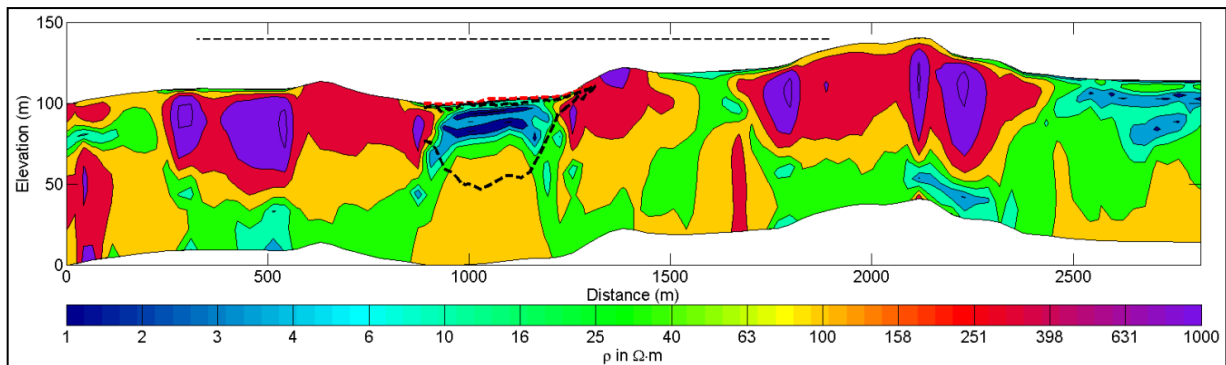


Figure 16 : Inverted model from five frequencies FHEM data along line -8 using UBC code with a starting model of $100 \Omega\text{m}$. Thicker dashed black lines show seismic velocity boundaries and dashed red line shows topography of seismic profile. Thinner dashed black line shows length and position of 2D resistivity survey profile.

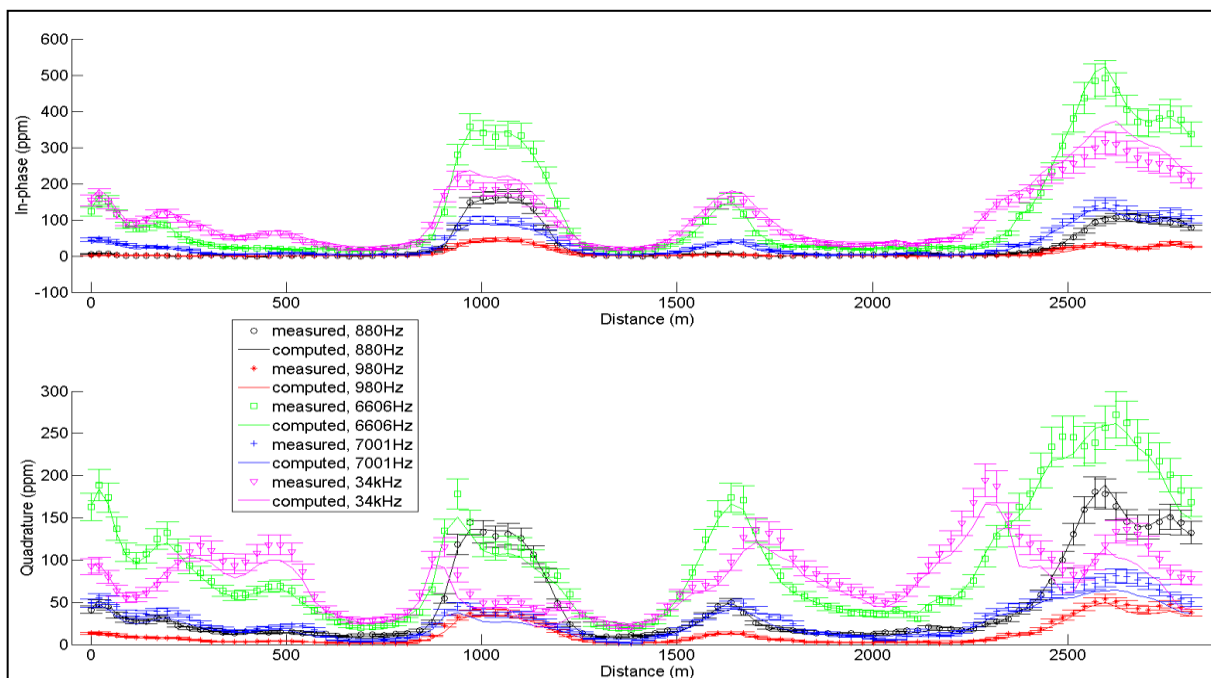


Figure 17: Fitting between measured FHEM data and computed data from inverted model obtained by UBC code along line -8. Symbols and solid lines represent measured and computed data for various frequencies, respectively.

Line 142 (Fig. 18) shows a top resistive layer (200–1000 Ωm) of approx. 20 m thickness with small conductive openings at 1600 m and 2000 m. A very conductive layer of approx. 1 Ωm lies below it which could be an unleached marine clay layer. However, interpretation of this resistive layer at the surface does not match with 2D resistivity and seismic data interpretation. Based on results from 2D resistivity and seismic refraction for same place and EM data at neighboring lines, the high resistivity at the upper part of this inverted line has to be wrong despite of good model fitting (Figure 19). We do not have a credible explanation for this.

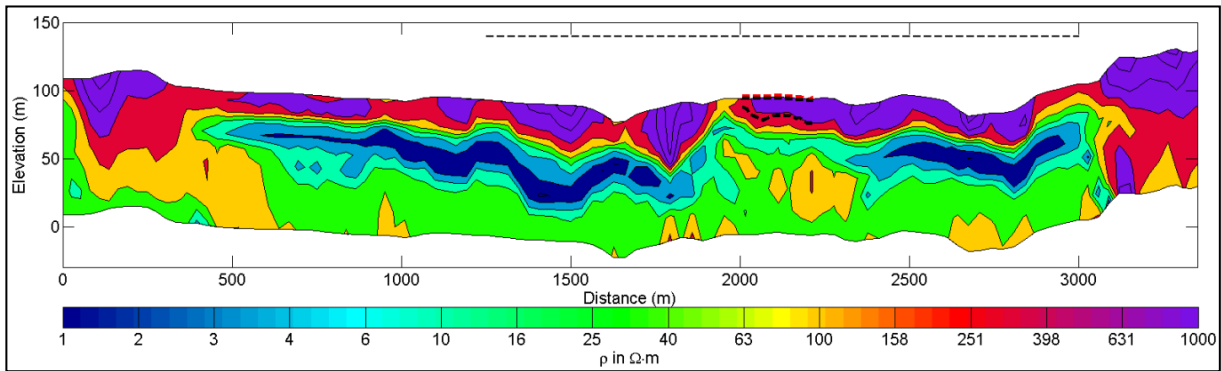


Figure 18: Inverted model from five frequencies FHEM data along line 142 using UBC code with a starting model of 100 Ωm . Thicker dashed black lines show seismic velocity boundaries and dashed red line shows topography of seismic profile. Thinner dashed black line shows length and position of 2D resistivity survey profile.

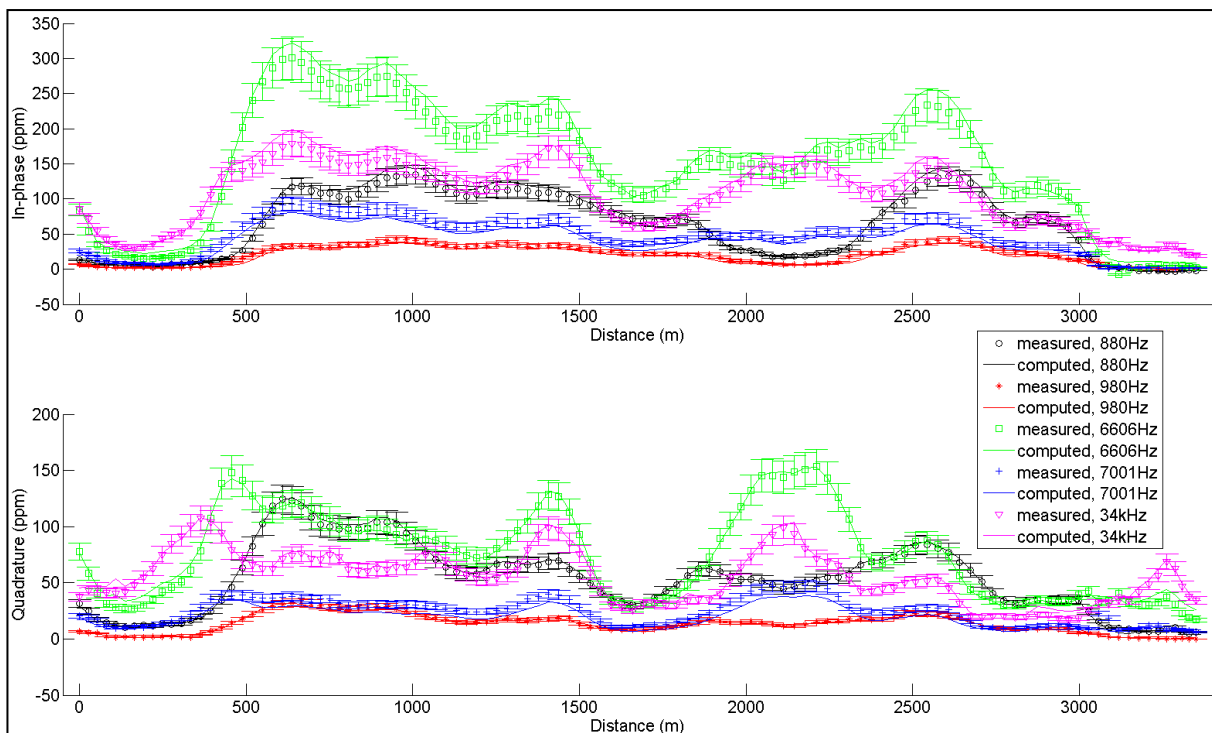


Figure 19: Fitting between measured FHEM data and computed data from inverted model obtained by UBC code along line 142. Symbols and solid lines represent measured and computed data for various frequencies, respectively.

Line 272 (Fig. 20) shows an approx. 20 m thick conductive layer of resistivity 1-10 Ωm with a surface layer of somewhat higher resistivity values. Seismic data was collected upto 200 m south of line 272 (Fig. 1) and suggest bedrock at 50 m below m.s.l. (approx. 130 m below surface). This interpretation is relatively close to the 2D resistivity data interpretation, but FHEM data suggests it shallower. However, as shown with the Aarhus inversion later, depth of investigation (DOI) is about 20 meters here, and deeper resistivity values are not reliable. Vertical low resistive structures at both ends (at 600 and 3300 m location) are probably artificial effects of 1D inversion. Figure 21 shows an overall good fitting of the inversion.

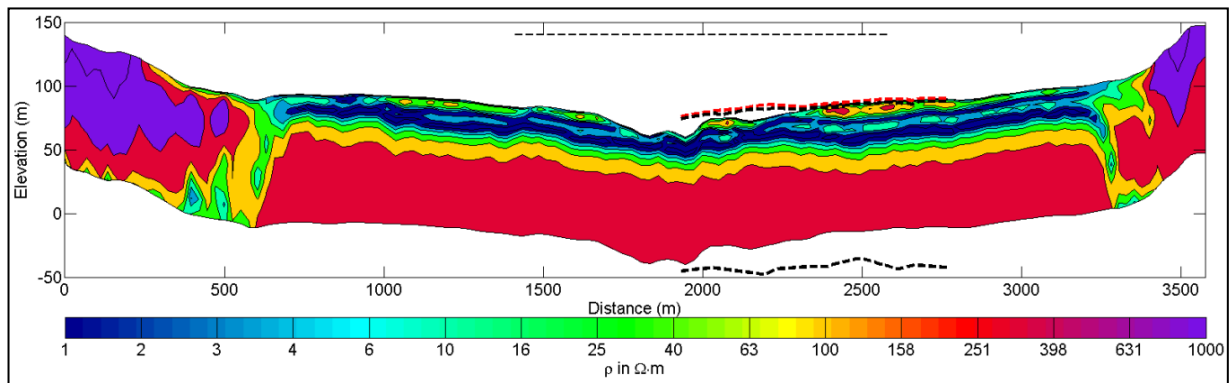


Figure 20: Inverted model from five frequencies FHEM data along line 272 using UBC code with a starting model of 100 Ωm . Thicker dashed black lines show seismic velocity boundaries and dashed red line shows topography of seismic profile. Thinner dashed black line shows length and position of 2D resistivity survey profile.

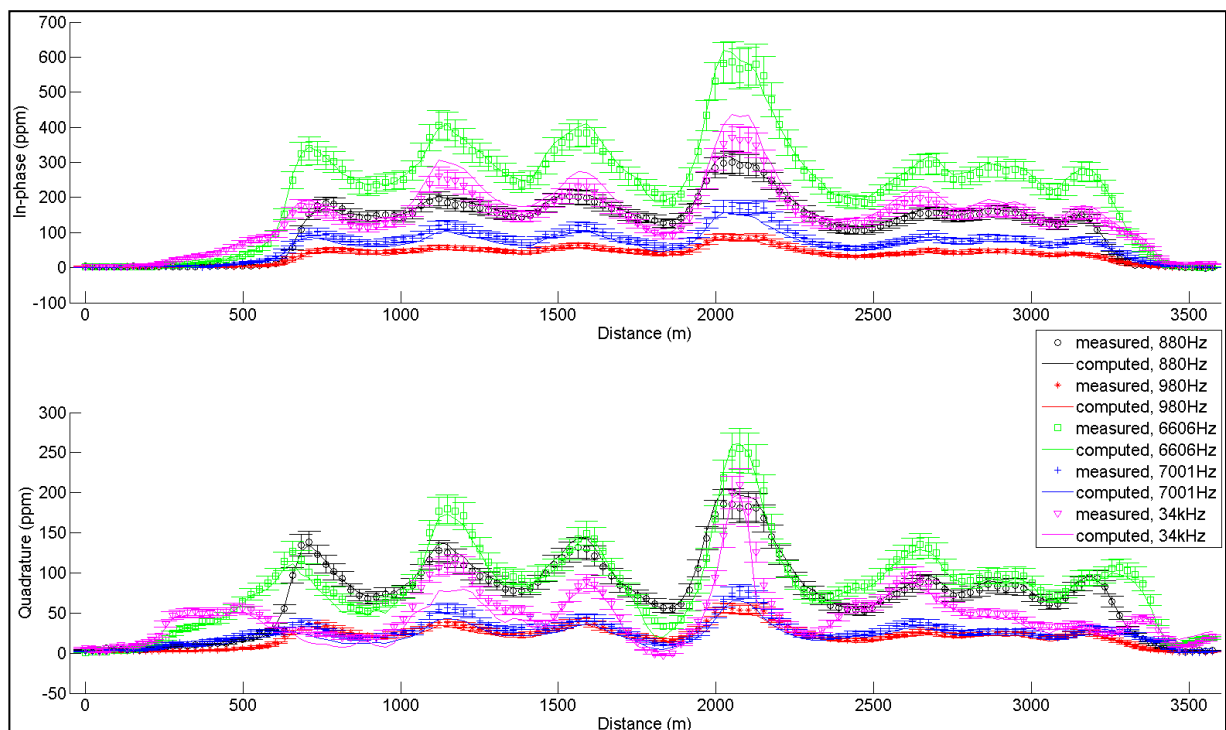


Figure 21: Fitting between measured FHEM data and computed data from inverted model obtained by UBC code along line 272. Symbols and solid lines represent measured and computed data for various frequencies, respectively.

Line 551 (Fig. 22) like line 272, shows a continuous layer of low resistivity values (1-10 Ωm), but here the surface layer is thicker and with higher resistivity value. It correlates relatively well with the 2D resistivity profiles. The bedrock is probably shallower here, than for profile 272. Figure 23 shows an overall good fitting from the inversion.

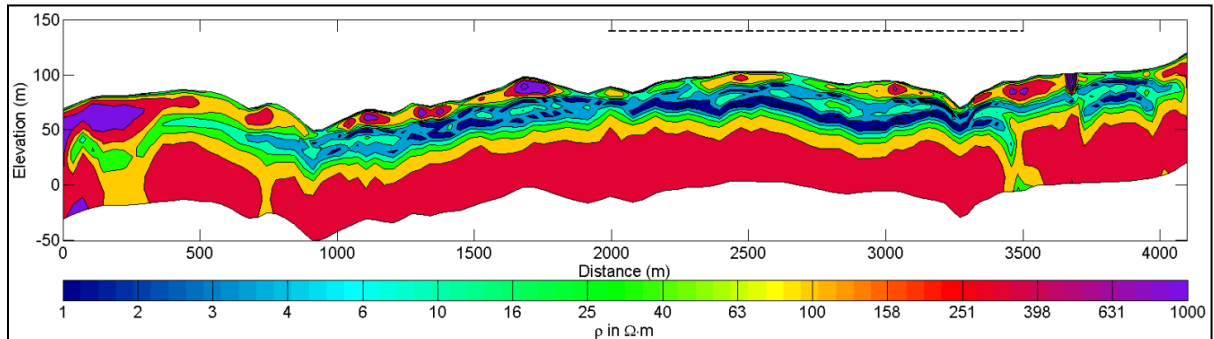


Figure 22: Inverted model from five frequencies FHEM data along line 551 using UBC code with a starting model of 100 Ωm . Dashed black line shows length and position of 2D resistivity survey profile.

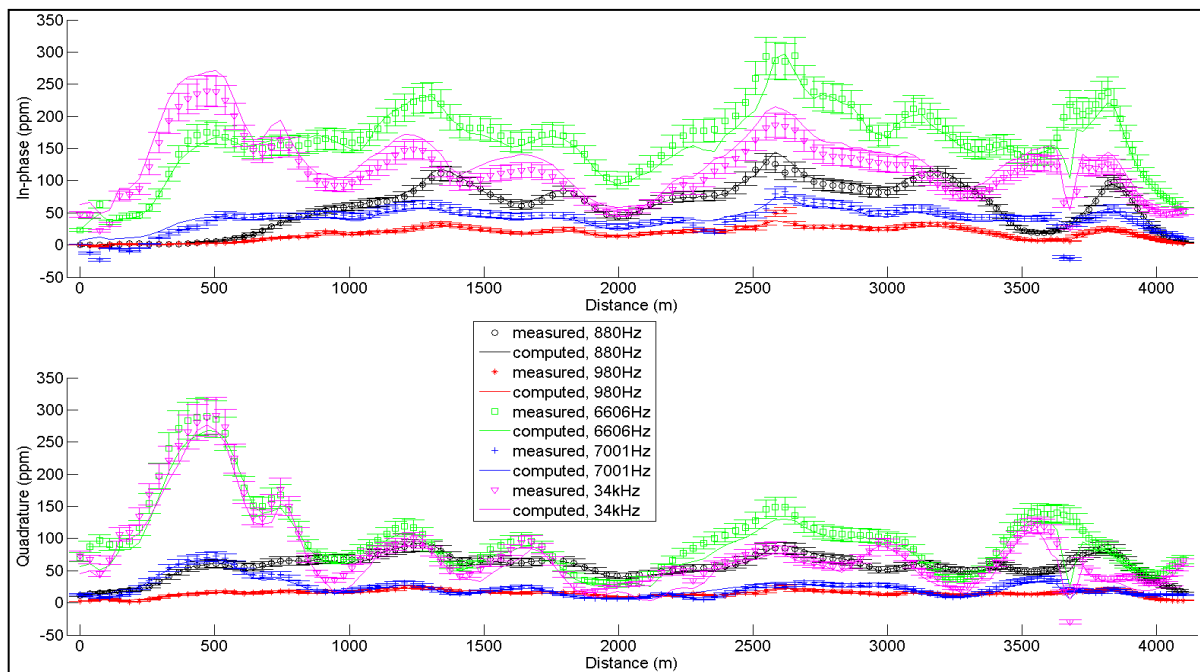


Figure 23: Fitting between measured FHEM data and computed data from inverted model obtained by UBC code along line 551. Symbols and solid lines represent measured and computed data for various frequencies, respectively.

3.3.2 Aarhus Constrained 1D inversion: AarhusInv

The AarhusInv (formerly called em1Dinv) is a program for inversion and analysis of electrical and electromagnetic methods applied in geophysical investigations. The program supports ground transient electromagnetic (TEM) systems, ground frequency domain electromagnetic (FEM) systems, ground direct current (DC) systems, airborne frequency and airborne time domain systems. The program performs one-dimensional (1D) inversion except in the case of DC data for which 2D responses are implemented. AarhusInv is easy to use and managed with the Aarhus Workbench as a graphical front-end, but can also be used as a stand-alone tool which is freely available for non-commercial purposes.

The basis of the code is a layered pseudo 3D model description and a local 1D forward response, which is used for computational feasibility. For most hydrogeological settings the spatial geological coherence of earth layers makes a 1D forward response an excellent approximation, especially when the geological coherency is further exploited to improve model resolution in the inversion. Hence, the code allows the user to specify any number of geological assumptions through an arbitrary combination of 3D coherence constraints and prior information. Inversion code considers sensor height also as one of the parameters and tries to correct the sensor height after few iterations of inversion. It calculates Depth Of Investigation (DOI) at the same time to provide some information about depth accuracy of the model (Christiansen and Auken, 2012). It can perform laterally and specially constrained inversions (LCI and SCI) by constraining physical properties of surrounding nodes/cells (Christiansen et al., 2007) to give a layered model unlike UBC's EM1DFM which inverts each data point separately to generate 1D model. Lateral/special constraints in Aarhus inversion code can sometime over-smooth the inverted model to impose the continuity of the layers and can even fail e.g. in mineral exploration where we are not looking for layered structures. So we have to apply correct setting required for the particular area depending on its known geology. There are lots of setting and facilities in Aarhus code in comparison to UBC code which can be used for a priori information. Details of the method are described by Auken and Christiansen (2004) and in the manual (AarhusInv, 2013).

First, few of the FHEM lines were inverted using LCI for a model containing 20 layers, 10 and 100 Ωm halfspaces and assuming 10 % standard noise in the data similar as for UBC inversion. Figure 24 depicts inverted model using LCI along line -8 from a starting model of 10 Ωm . The inverted model is plotted in Aarhus workbench. DOI was also calculated and plot is faded below lower DOI level. Data residual is shown by red rectangles and lines. DOI level suggests that approx. 20 m depth is reliable in conductive areas even with a good data fitting in this profile and it can be deeper in resistive areas. Inverted altitude (purple rectangles) shows deviation of around 10 m with measured altitude (green rectangles) which could be true due to false height observed by radar altimeter from top of the trees instead of ground surface (canopy effect) and inaccuracy in the radar altimeter data.

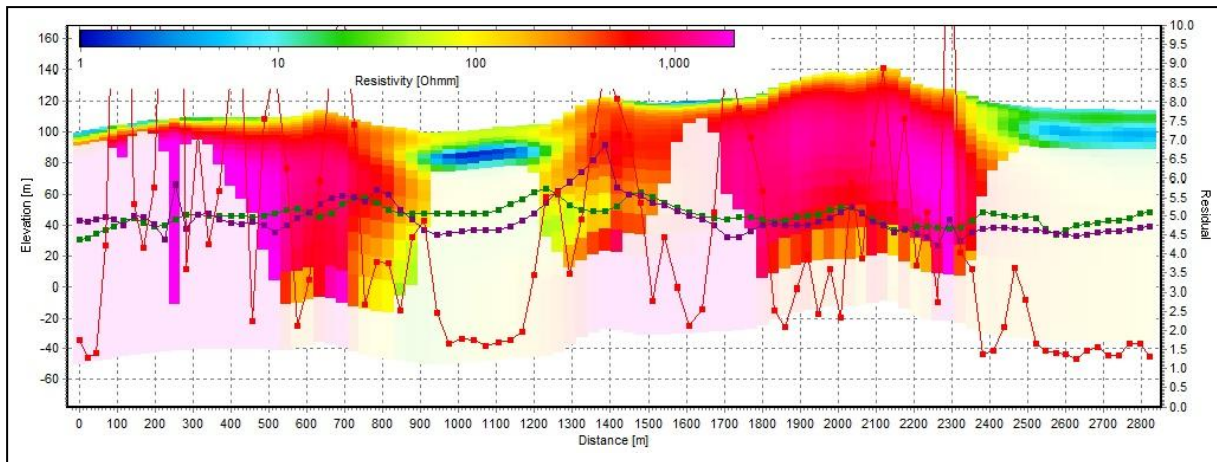


Figure 24: Inverted model from five frequencies FHEM data along line -8 using LCI of Aarhus code with a starting model of 10 Ωm . Green and purple line/symbols represent measured and computed altitude, respectively. Red line/symbol represents data residual. Fading of the image is done to show depth of investigation (DOI).

Same inverted result is shown in Fig. 25 using Matlab for comparison using the color scale (Fig. 2) as used for 2D resistivity model and UBC's FHEM model. We also tried another inversion by setting standard deviation in sensor altitude to 2 m (instead of 3 m before), vertical constraint to be 3 (instead of 5 before) and starting model to be 100 Ωm (instead of 10 Ωm) and obtained a less smooth image of the subsurface as shown in Fig. 27. Fitting in the data is almost similar for both of these models and are shown in Figs. 26 and 28. We can observe that UBC inverted model shows a better fitting for the same data (Fig. 17). However, both the inversion codes suggest broadly similar conductive structures along Line -8 (especially above DOI level).

One of our aims was to compare results of FHEM inversion from UBC and Aarhus codes therefore we inverted FHEM data along line 142, 272 and 551 using LCI method and with a starting model of 100 Ωm to compare it with inverted models obtained from the UBC code. However, we will not show inverted models and data fitting for these EM lines individually rather, we will show inverted models using AarhusInv along these lines together with inverted models from UBC code and 2D Resistivity data for an easy comparison in the next section.

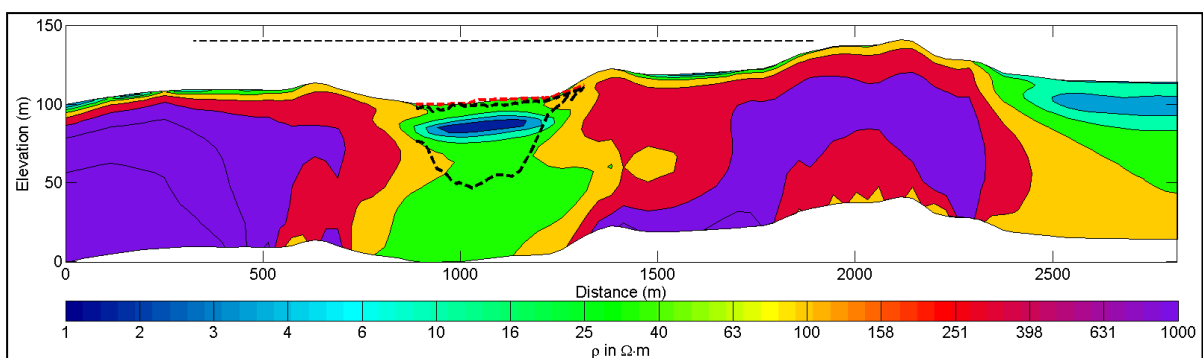


Figure 25: Inverted model from five frequencies FHEM data along line -8 using LCI of Aarhus code with a starting model of 10 Ωm (same as shown in Fig. 24 however plotted in Matlab). Thicker dashed black lines show seismic velocity boundaries and dashed red line shows topography of seismic profile. Thinner dashed black line shows length and position of 2D resistivity survey profile.

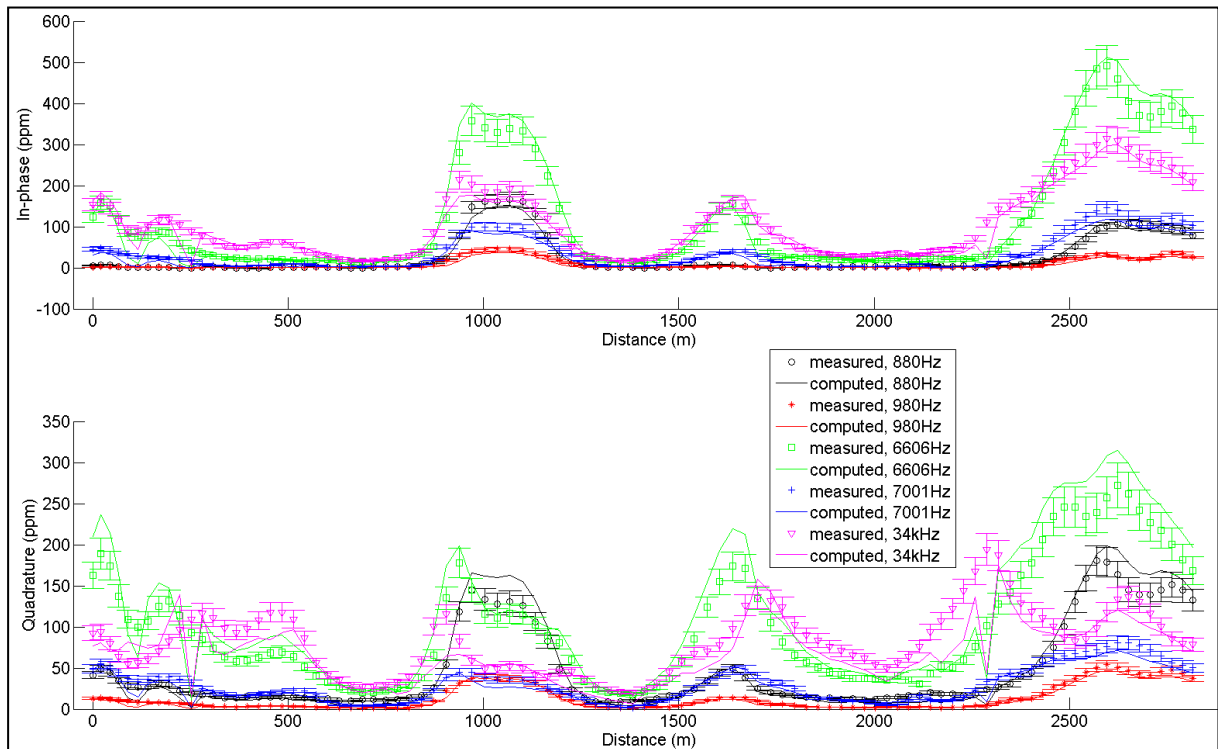


Figure 26: Fitting between measured FHEM data and computed data from inverted model obtained by LCI of Aarhus code along line -8 with a starting model of 10 Ωm . Symbols and solid lines represent measured and computed data for various frequencies, respectively.

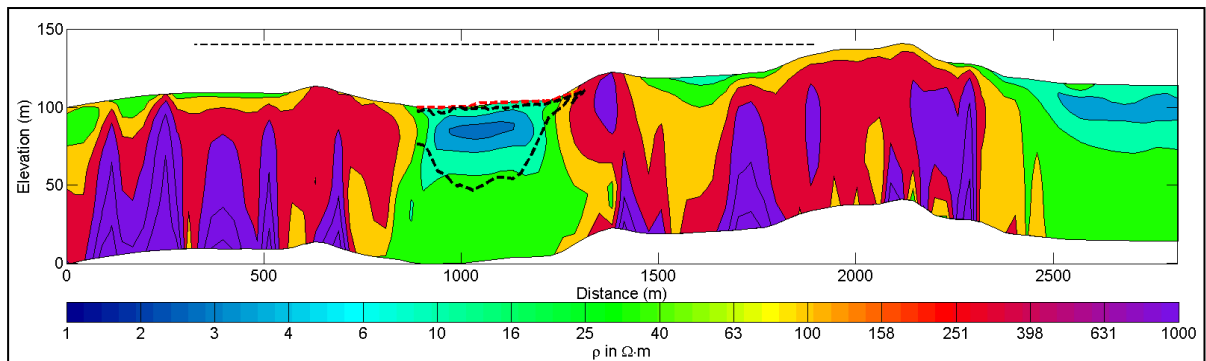


Figure 27: Inverted model from five frequencies FHEM data along line -8 using LCI of Aarhus code with a starting model of 100 Ωm and with different settings. Thicker dashed black lines show seismic velocity boundaries and dashed red line shows topography of seismic profile. Thinner dashed black line shows length and position of 2D resistivity survey profile.

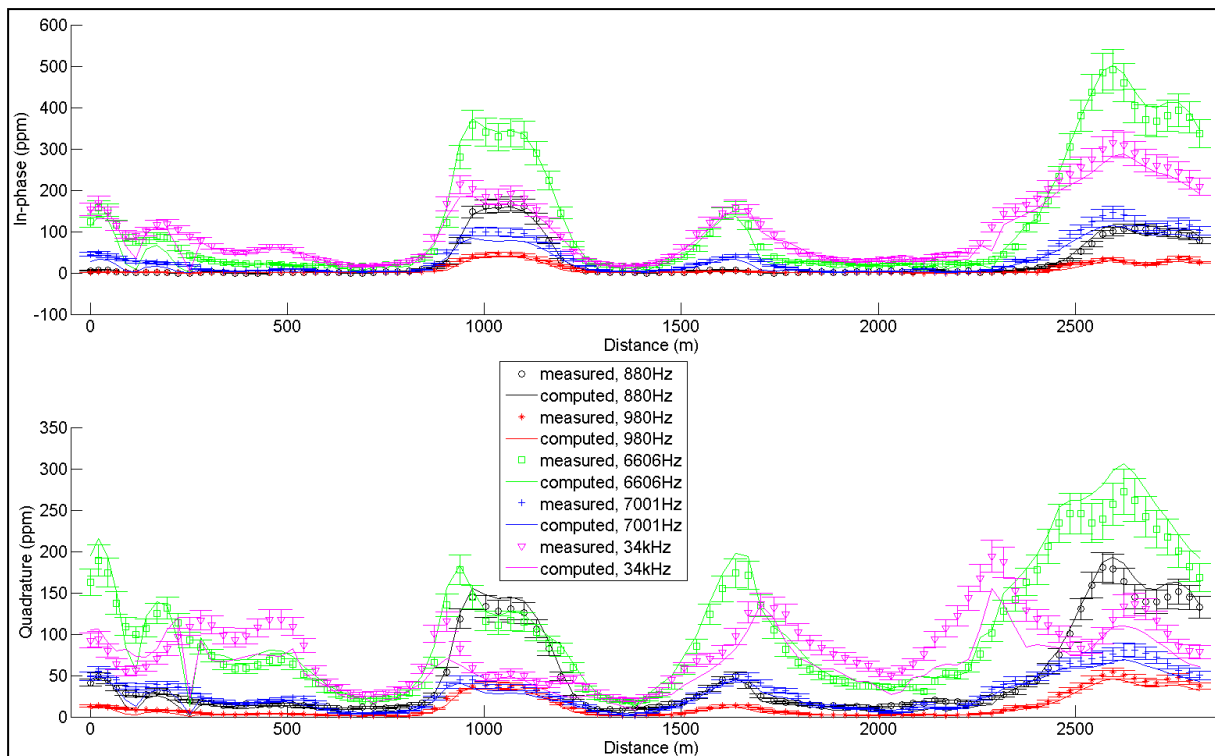


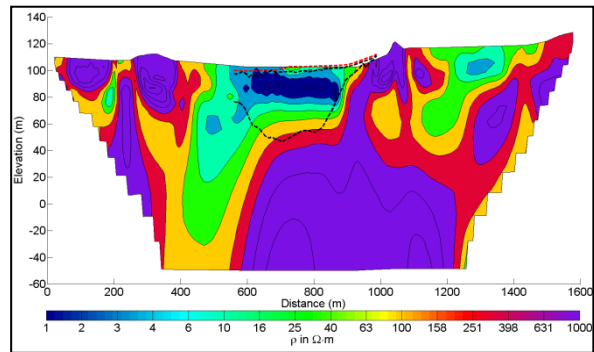
Figure 28: Fitting between measured FHEM data and computed data from inverted model obtained by LCI of Aarhus code along line -8 with a starting model of 100 Ω m. Symbols and solid lines represent measured and computed data for various frequencies, respectively.

3.3.3 Comparison of inverted 2D resistivity and FHEM models

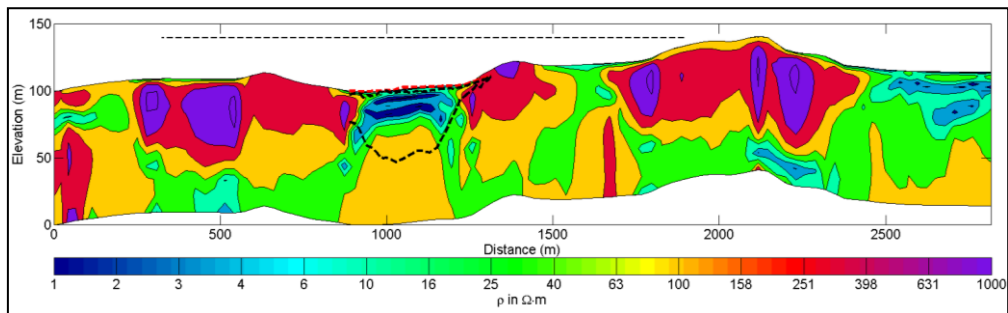
Figure 29 presents inverted models from 2D resistivity and FHEM data together along line -8. Top layer conductive areas in FHEM models are interpreted at similar locations by both UBC and AarhusInv codes (Figs. 29b and c). However, UBC code interprets moderate resistivity at bottom in contrast to high resistivity by AarhusInv code. Bedrock layer location shown by seismic refraction is in good agreement to 2D resistivity interpretation (Fig. 29a) but not predicted well by FHEM data.

Figure 30c presents inverted FHEM model using AarhusInv along line 142, which is quite different than what obtained from UBC code (Fig. 30b). There is no top resistive layer in inverted model as indicated by UBC model rather it is a moderate resistive layer. This moderate resistive layer also suggested by 2D resistivity (Fig 30a) could be a quick clay layer. Seismic refraction data had suggested bedrock starting around 50 m below surface. However, FHEM data could not see any bedrock even at 100 m depth below surface which could be either due to skin depth limitation as discussed before or bedrock containing conductive minerals (Solberg et al., 2015).

(a)



(b)



(c)

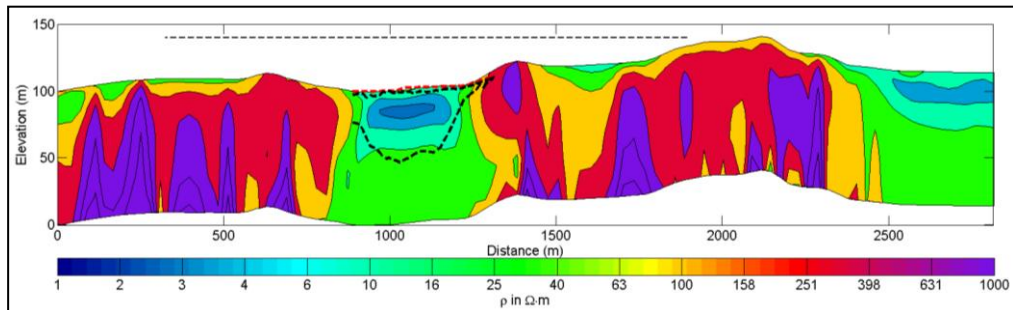
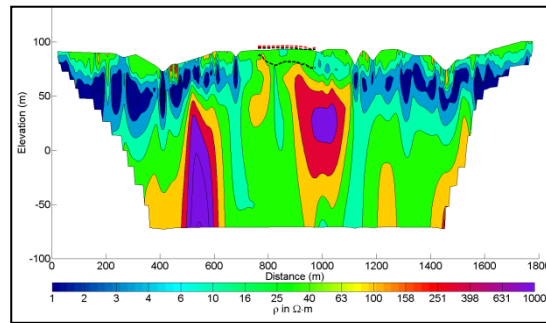
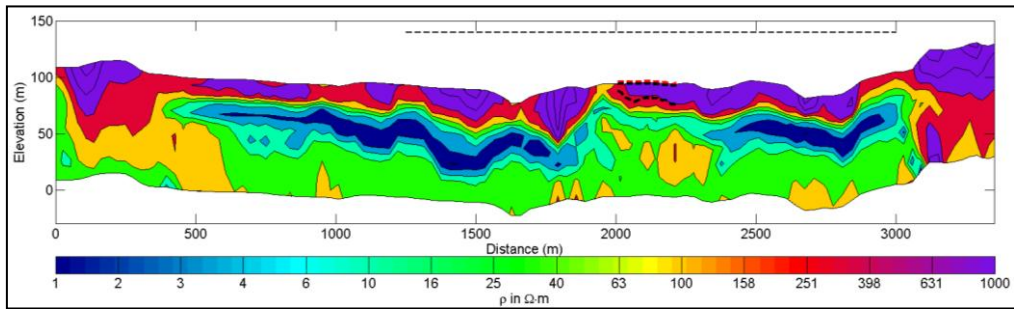


Figure 29: (a) Inversion results from 2D resistivity data, (b) FHEM data using UBC code, and (c) inverted model from five frequencies FHEM data along line -8 using LCI of Aarhus code with a starting model of 100 $\Omega\cdot m$. Thicker dashed black lines show seismic velocity boundaries and dashed red line shows topography of seismic profile. Thinner dashed black line shows length and position of 2D resistivity survey profile.

(a)



(b)



(c)

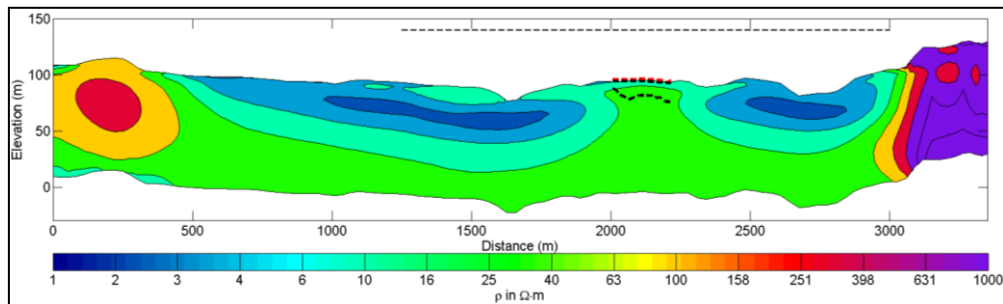
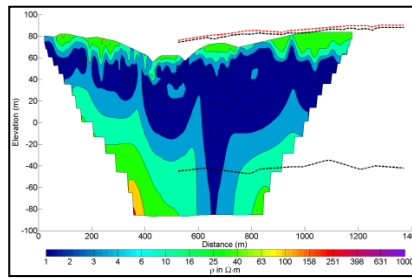


Figure 30: (a) Inversion results from 2D resistivity data, (b) FHEM data using UBC code and (c) inverted model from five frequencies FHEM data along line 142 using LCI of Aarhus code with a starting model of 100 $\Omega \cdot m$. Thicker dashed black lines show seismic velocity boundaries and dashed red line shows topography of seismic profile. Thinner dashed black line shows length and position of 2D resistivity survey profile.

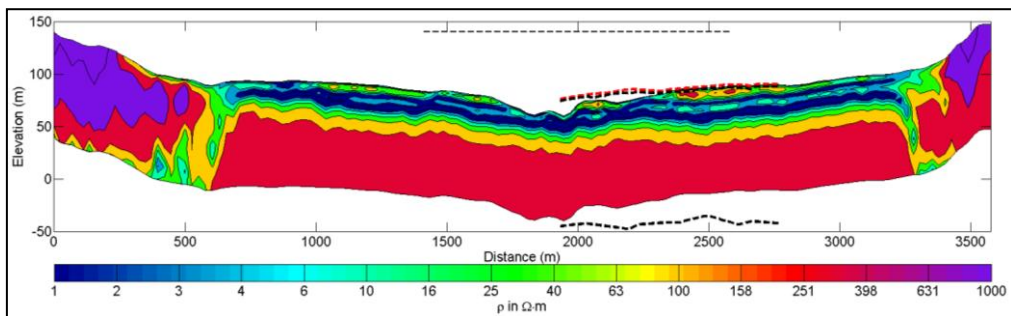
Figures 31 and 32 depict inverted models for line 272 and 551, respectively. Both models suggest a moderate conductive layer (10-50 Ωm) at the top which can be interpreted as possible quick clay or silty sediment and a conductive layer of around 1 Ωm below it at approx. 20 m below the surface. Inversion using UBC code and inversion of 2D resistivity data has also suggested similar interpretation however depth of bedrock is interpreted differently. Fitting of the measured data with computed/synthetic response of inverted model for FHEM data is always better for models generated by UBC code than Aarhus code. This could be explained by two reasons as (1) UBC code is inverting each data point separately without considering neighboring data points and hence it produces rather irregular structure with good fitting while Aarhus code considers neighboring data and continuity so produces a rather regular structure with relatively bad data fitting (2) Better data fitting for UBC model may also indicate that inverted model is not as smooth as it is shown by LCI of AarhusInv.

We performed various runs of LCI to investigate the controlling factor for data fitting in LCI and found that lateral and vertical constraints had less dominance over sensor altitude in controlling the data fitting. We got similar data fitting and non-smooth models with almost no constraints. However, when we allowed altitude to vary, then it produced better data fitting for even smooth models. We observed that inverted models obtained from 10 Ωm starting model (not shown here for all the lines) were close to the inverted models obtained from 2D resistivity data. Inversion by AarhusInv along some of the lines was even failed when we tried to invert it with 100 Ωm starting model. Resistivity of 10 Ωm is closer to the resistivity of the fresh marine clay layers (< 10 Ωm) which is very conductive. This could be one of the reasons for stability of the AarhusInv for starting model of 10 Ωm . We chose 10 Ωm starting model when we performed SCI for all the FHEM lines as discussed in the next section.

(a)



(b)



(c)

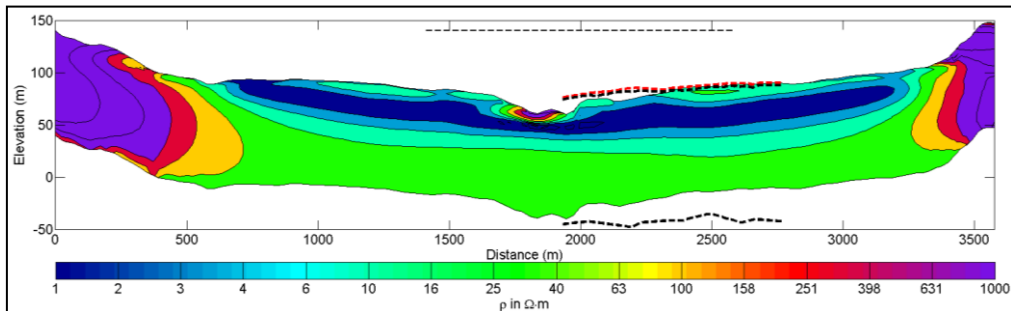
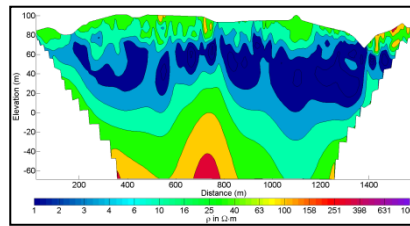
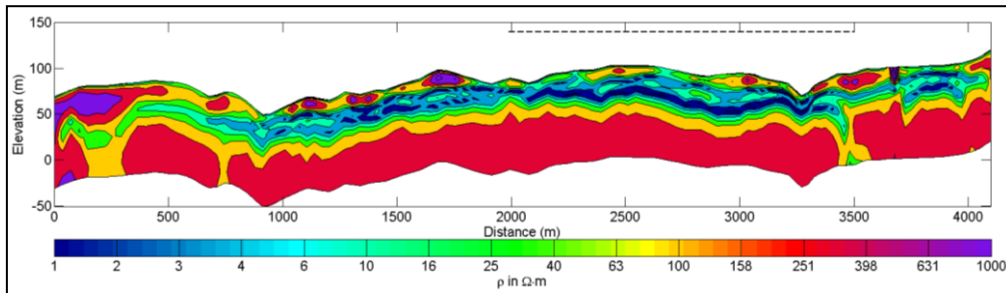


Figure 31: (a) Inversion results from 2D resistivity data, (b) FHEM data using UBC and (c) inverted model from five frequencies FHEM data code along line 272 using LCI of Aarhus code with a starting model of $100 \Omega\text{m}$. Thicker dashed black lines show seismic velocity boundaries and dashed red line shows topography of seismic profile. Thinner dashed black line shows length and position of 2D resistivity survey profile.

(a)



(b)



(c)

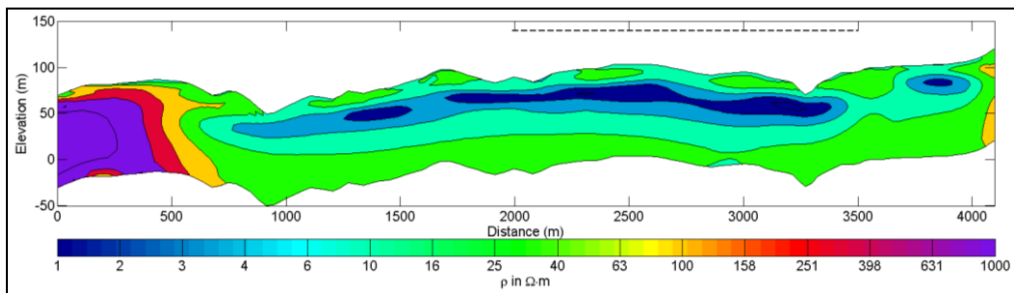


Figure 32: (a) Inversion results from 2D resistivity data, (b) FHEM data using UBC code and (c) inverted model from five frequencies FHEM data along line 551 using LCI of Aarhus code with a starting model of 100 Ω·m. Dashed black line shows extent of 2D resistivity survey profile. Dashed black line shows length and position of 2D resistivity survey profile.

3.4 3D presentation of inverted data

In this chapter, we present 3D models obtained from inversion of all FHEM data using SCI (Spatial Constrained Inversion) of AarhusInv code.

3.4.1 Stacked profiles and horizontal slices

FHEM data was collected along flight lines -8 to 681 covered in 60 lines with line spacing of 100 m in north and 200 m for few lines in south (Fig. 1). FHEM data were averaged using a running average of 10 points to produce data at approx. 30 m interval along flight lines and inverted all together using SCI of AarhusInv code. A homogenous model of 10 Ωm with 20 layers of total 100 m thickness was used as starting model for the inversion. Lateral and vertical constraints were set as 1.3 and 3, respectively. In this way, we could perform a sort of 3D inversion to obtain a 3D resistivity image of the surface. However, the long lateral distance of 100 to 200 m across flight lines and approx. 30 m data spacing along the flight line was not ideal.

Matlab and Geosoft were used to plot a 3D image of subsurface resistivity as shown in Figs. 33 and 34, respectively. It was not possible to interpolate resistivity three-dimensionally in Matlab therefore they were plotted as a wireframe diagram along the flights lines (Fig. 33). Inverted resistivity was gridded using the inverse distance method in Geosoft for various depths below ground (i.e. 0, 2, 5, 9, 14, 21, 25, 31 m) and a sliced image of the subsurface is shown in Fig. 34. The inverted model shows that the surveyed area is surrounded by high resistive structures and some of them even outcrop in middle of northern part of the surveyed area. The central region of the area is conductive without outcropping of high resistive features. It comprises of a thin and moderately resistive (10-100 Ωm) layer of possible quick clay or silty sediments with fresh and unleached marine clay (< 10 Ωm) underneath. In the central part, the unleached marine sediments are thicker and it is not possible to interpret bedrock depth correctly by FHEM data. Even the interpreted resistivity values shown at 40-50 m depth and below the conductive layer do not seem to be correct as we explained earlier due to a low DOI and skin depth in such areas. This depth limitation of FHEM interpretation was evident when we compared FHEM results with 2D resistivity and refraction seismic results.

We also tried to plot a 3D image of resistivity by interpolating it in Geosoft instead of making only slices. We tried direct gridding, weighted inverse distance and kriging methods for the gridding. We could do gridding assuming minimum 5 m vertical cell for this large model. We observed that thin horizontal layers of 10-100 Ωm resistivity disappeared in the interpolation when we used inverse distance and kriging method. It was well visible in direct gridding method where vertical 2D subsurface (in x and z direction) were created along flight lines. Therefore, we did not use 3D interpolation of Geosoft to present iso-surfaces of particular resistivity zones/clay layers.

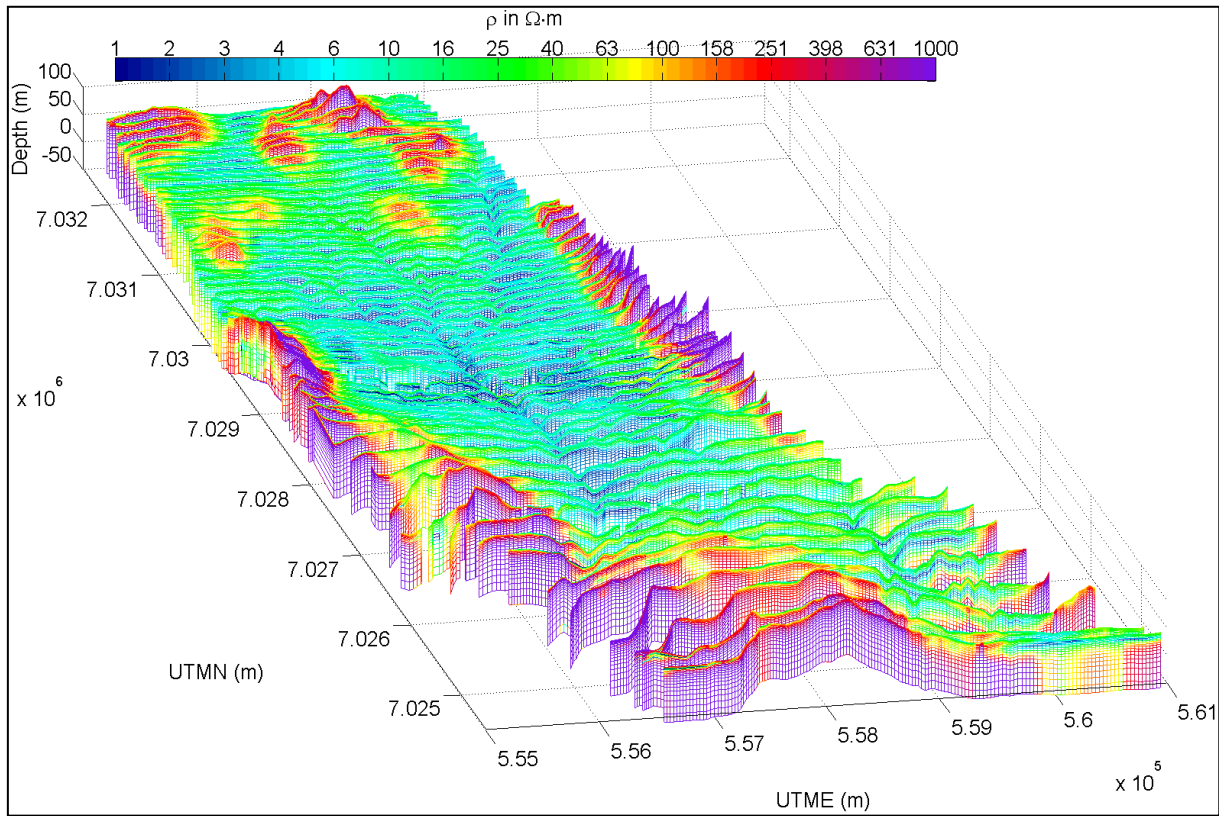


Figure 33: 3D resistivity image plot in Matlab from inversion of FHEM data. Inverted resistivity was obtained using SCI inversion of AarhusInv code with a starting model of 10 Ωm .

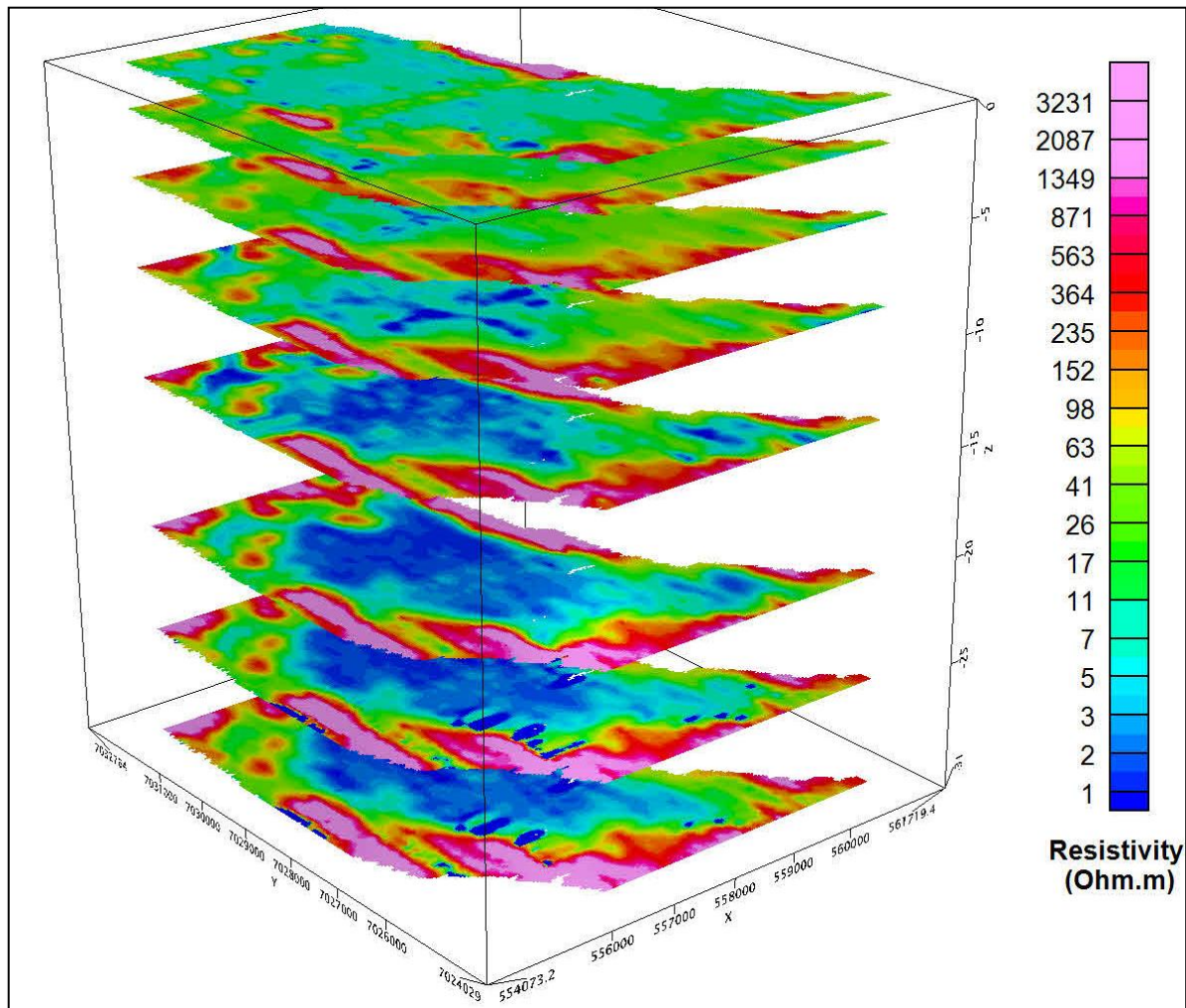


Figure 34: 3D slices of resistivity image from 0 m to 30 m depth below surface plotted in Geosoft and extracted from inversion of FHEM data as shown in Fig. 33.

Following the classification by Solberg et al. (2008) as shown in Fig. 2 and the comparison of refraction seismic, 2D resistivity and FHEM data, we plotted resistivity layer at 1 m depth below ground as shown in Fig. 35. Location of exposed bedrock and geotechnical drillings are shown by black circle and triangles, respectively. Dark yellow to pink colour represents resistivity above 100 Ωm interpreted as coarse sediments, sand, gravel and bedrock. Green to light yellow represents resistivity between 10 to 100 Ωm interpreted as leached clay which may contain quick clay. Light to dark blue represents resistivity below 10 Ωm to indicate unleached and stable clay.

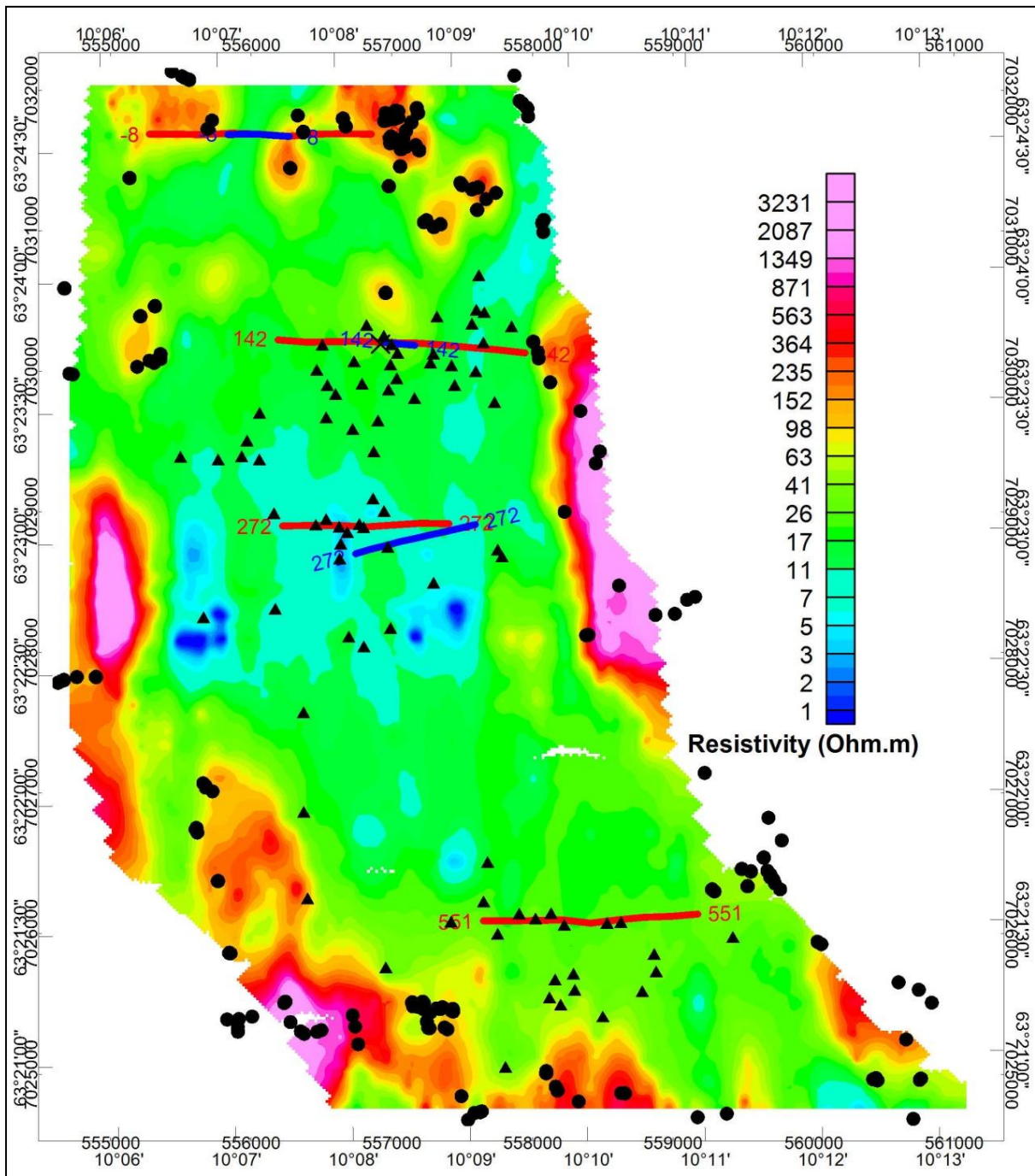


Figure 35: Resistivity image at 1 m depth obtained by SCI inversion of FHEM data with a starting model of 10 Ω m (from same image shown in Fig. 33). Black dots and black triangles represent exposed bedrock and geotechnical drilling locations, respectively. Red and blue lines represent 2D resistivity and seismic refraction profiles, respectively.

3.4.2 Depth to bedrock

We further tried to extract bedrock depth information from inverted resistivity model from FHEM data. Though there was low EM signal and bad data fitting in hard rock areas, it gave an indication about exposed and close-to-surface bedrock locations. However, the depth estimation may not be very accurate. We need to incorporate borehole resistivity results to verify and adapt it for better accuracy.

Generally, bedrock has very high resistivity in order of few hundreds to few thousands Ωm . We observed relatively lower resistivity from FHEM data in this area. Electronic conductive minerals (e.g. graphite) have been reported in the bedrock from this area (Solberg et al., 2015) which could be one of the reasons for low resistivity of the bedrock. Therefore, we extracted all the locations having top layer greater than a particular resistivity (say 100 Ωm) and plotted the depth of this layer. DOI was also considered in the plotting because it tells how much depth has reliability in the interpretation of FHEM data. When depth of these layers was found deeper than DOI, then DOI was used as the minimum bedrock depth in the plotting instead of their interpreted depth.

Figs. 36-38 show depth to bedrock for resistivity $> 500 \Omega\text{m}$, $> 200 \Omega\text{m}$ and $> 100 \Omega\text{m}$, respectively for indicating top layer of the bedrock. We also plotted four locations (bigger coloured circle) where bedrock depth was known by the earlier drilling (from quaternary map on NGU website). These circles are plotted with same colour scale for the depth as shown in the figures and show a good agreement with interpreted bedrock depth by FHEM data. We observed that some of the observed exposures are not covered in the grid having resistivity $> 500 \Omega\text{m}$ in Fig. 38. Resistivity of 100 Ωm is observed for dry crust clay and coarse sediments and it is too low to be accounted for the bedrock resistivity. Therefore we considered $> 200 \Omega\text{m}$ to represent the bedrock as shown in Fig. 37. Considering a resistivity of 200 Ωm for bedrock is also supported from 2D resistivity survey interpretation when compared with seismic refraction interpretation as we discussed in section 3.1.2. The plot in Fig. 37 is further simplified to fewer colours and limited to approx. 25 m depth below surface as shown in Fig. 39.

It is important to note that the hollow region in the middle should be interpreted with either deeper or uncertain bedrock depth. FHEM data was not able to resolve resistivity of the structure below the 20-40 m in thick conductive regions (as shown by DOI calculation) and interpreted it as continuation of conductive material. FHEM has shown a resistivity of approx. 30 Ωm below these depths in some regions, which is not true as shown in comparison of refraction seismic and FHEM models along line L -8 and L 142 (Figs. 29 and 30).

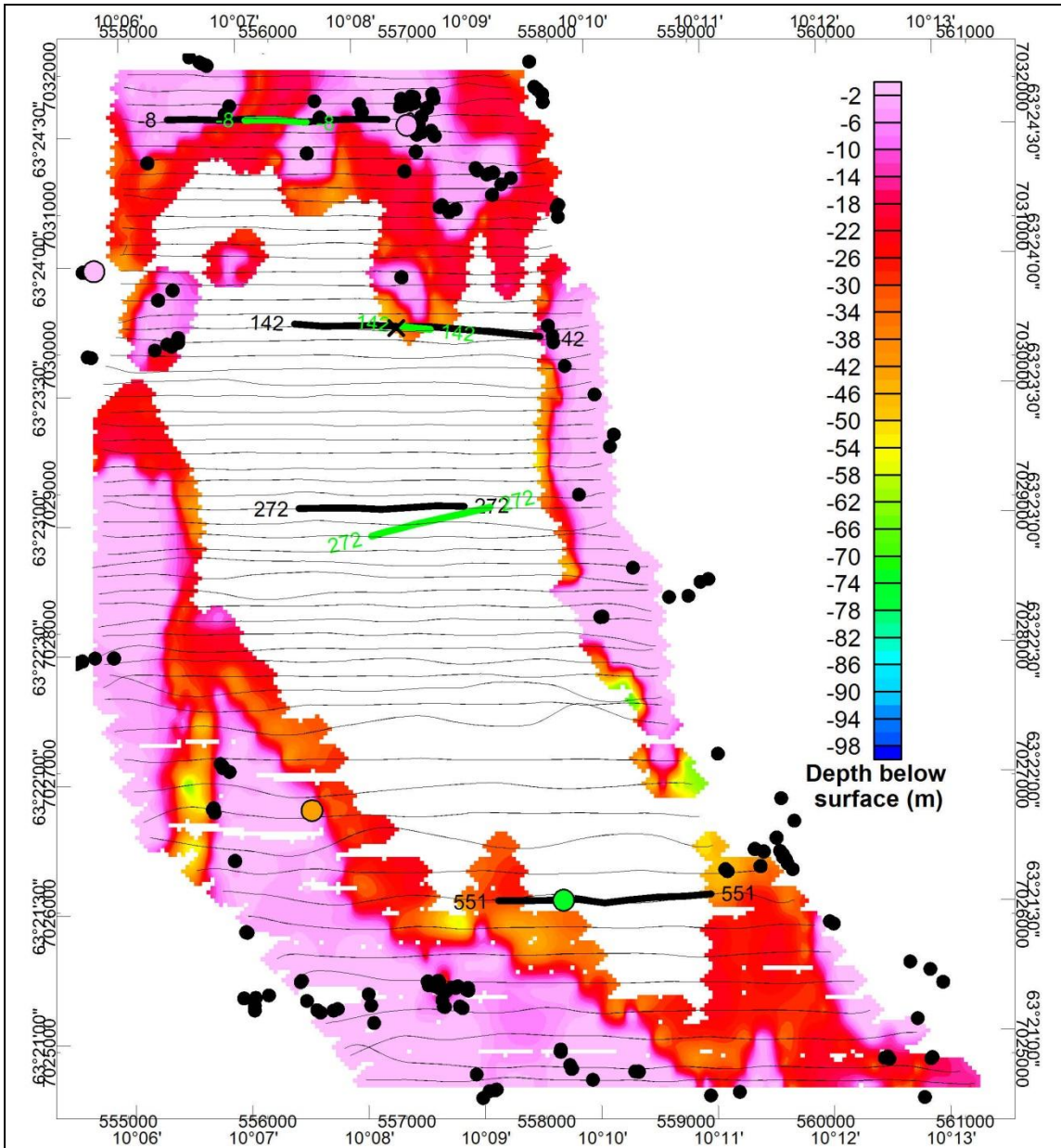


Figure 36: Depth of a resistivity zone $> 100 \Omega\text{m}$ deduced from SCI inversion of FHEM data as shown in Fig. 33. Black dots represent exposed bedrock locations. Thin black, thicker black and green lines represent FHEM, 2D resistivity and seismic refraction lines, respectively. Coloured circles show bedrock depth confirmed by drilling. White areas in centre of the map represent depth to bedrock deeper than 30 m.

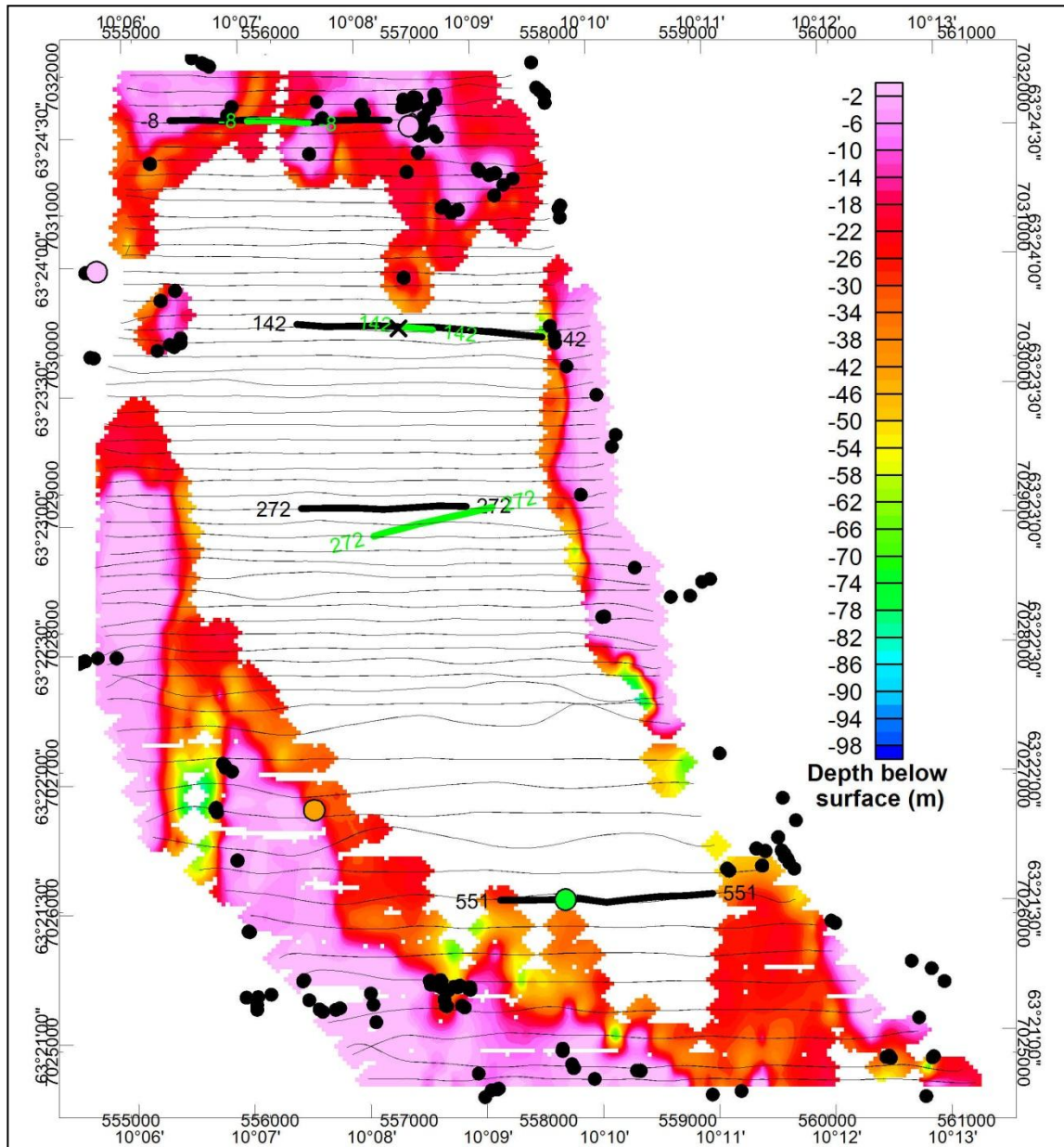


Figure 37: Depth of a resistivity zone $> 200 \Omega\text{m}$ deduced from SCI inversion of FHEM data as shown in Fig. 33. Black dots represent exposed bedrock locations. Thin black, thicker black and green lines represent FHEM, 2D resistivity and seismic refraction lines, respectively. Coloured circles show bedrock depth confirmed by drilling. White areas in centre of the map represent depth to bedrock deeper than 30 m.

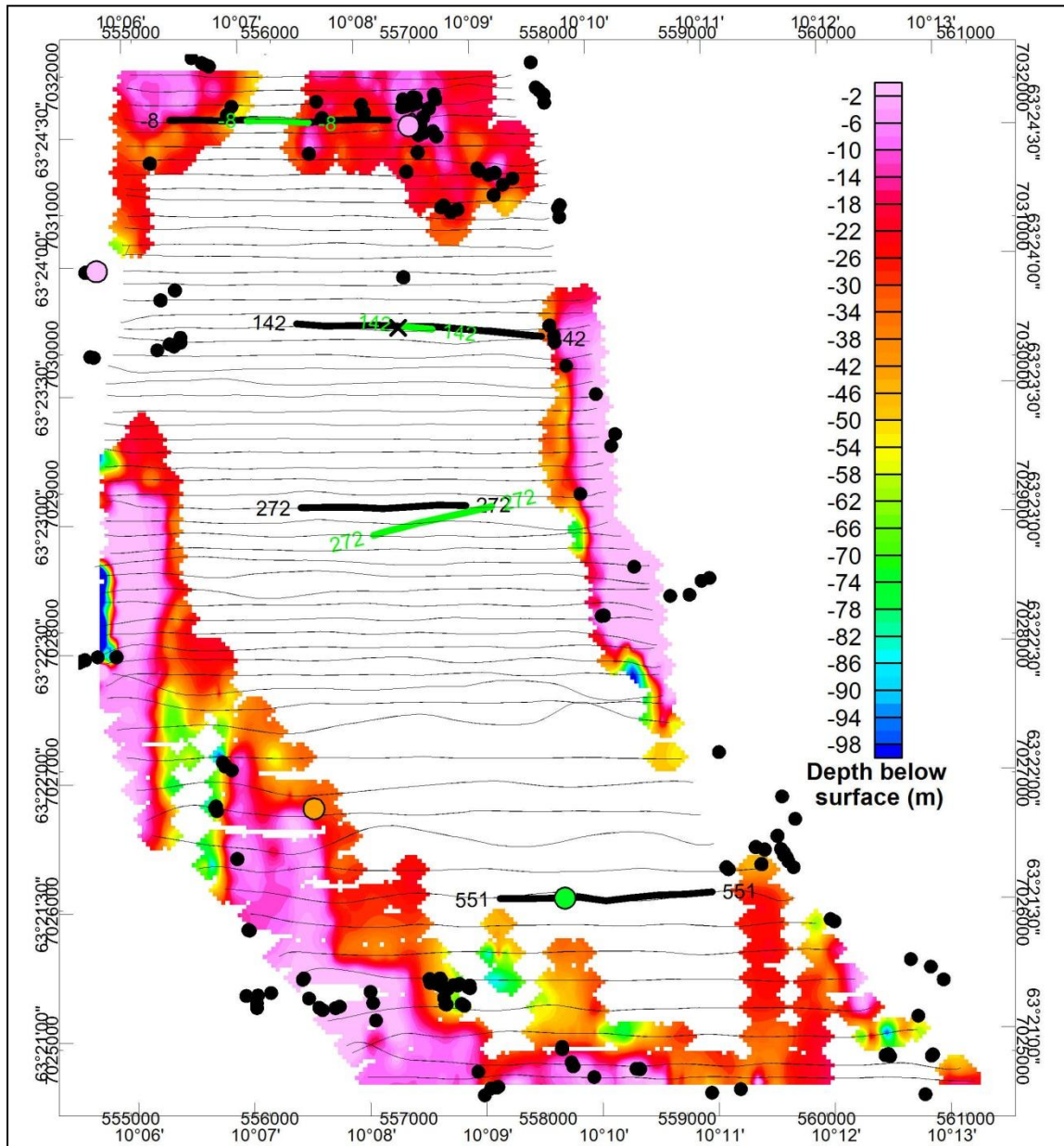


Figure 38: Depth of a resistivity zone $> 500 \Omega\text{m}$ deduced from SCI inversion of FHEM data as shown in Fig. 33. Black dots represent exposed bedrock locations. Thin black, thicker black and green lines represent FHEM, 2D resistivity and seismic refraction lines, respectively. Coloured circles show bedrock depth confirmed by drilling. White areas in centre of the map represent depth to bedrock deeper than 30 m.

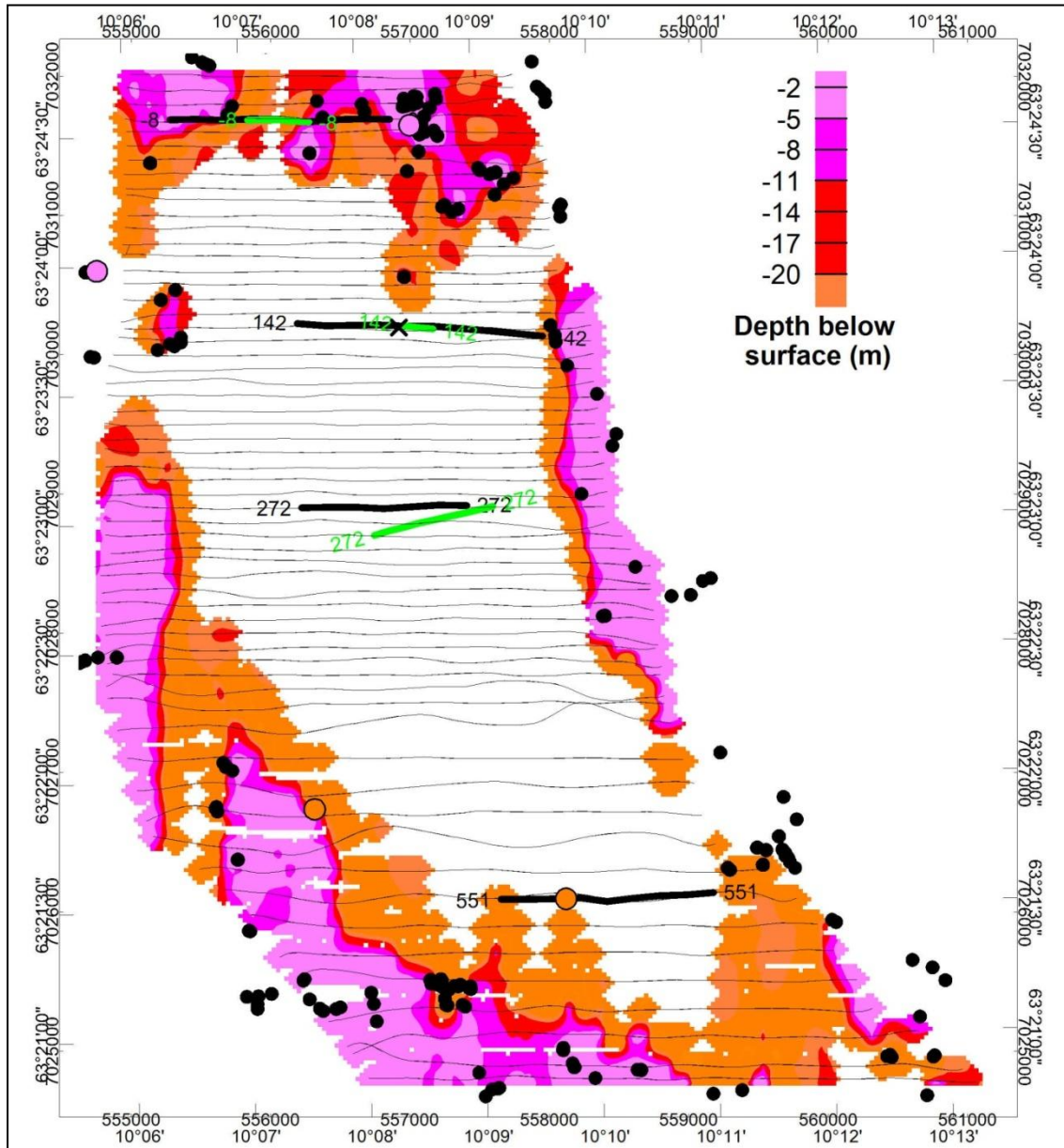


Figure 39: Modified plot of depth restricted to approx. 25 m and use of fewer colors for resistivity zone $> 200 \Omega\text{m}$ as shown in Fig. 37. $200 \Omega\text{m}$ was assumed as an indication of bedrock resistivity. Black dots represent exposed bedrock locations. Thin black, thicker black and green lines represent FHEM, 2D resistivity and seismic refraction lines, respectively. Coloured circles show bedrock depth confirmed by drilling. White areas in centre of the map represent depth to bedrock deeper than 30 m.

3.4.3 Comparison of resistivity data towards the depth

There were two locations (2 and 11, Fig. 1) where downhole resistivity was measured by RCPTu (Montafia, 2013; Hundal, 2014). We selected two more locations (A and 202, Fig. 1) from geotechnical drillings where we have FHEM and 2D resistivity data at relatively closer distance. Locations of these points are shown by black diamond with their names in Fig. 1. Table 4 shows their coordinates and distance from nearest FHEM and 2D resistivity measurements.

Table 4: Location of RCPTu and geotechnical drilling and their distance from FHEM and 2D resistivity measurements.

BoreHole ID	UTME_32	UTMN_32	Distance from nearest FHEM data point (m)	Distance from nearest 2D resistivity data point (m)
11	557004	7030140	25	70
2	556787	7029902	6.3	-
A	556458	7028898	5.2	8.4
202	556768	7028902	4.6	9.1

Resistivity values at these locations are extracted from SCI inverted FHEM model and 2D resistivity model. They are plotted together with resistivity from RCPTu and interpreted clay types from geotechnical drilling (Solberg et al., 2015) as shown in Figs. 40-43. Resistivity from RCPTu, FHEM and 2D resistivity survey are shown by green, black and red colored lines, respectively. Boundaries for interpreted clay types are presented by blue cross along with abbreviation for various clay types where LC, QC and UC represent leached clay, possible quick clay and unleached clay, respectively. Dashed vertical line represents 10 Ω m boundary to separate unleached and leached clay. Dashed horizontal line represents DOI for FHEM data.

Figure 40 shows the plot for drilling location 11. Resistivity obtained from RCPTu and FHEM data are shown but no resistivity from 2D resistivity survey because nearest 2D resistivity measurement point is approx. 70 m far. We see a surprisingly good agreement between resistivity from RCPTu and FHEM. FHEM data could not interpret top resistive layer (down to 2 m) well as shown by RCPTu which might be due to the fact that highest frequency of FHEM is 34 kHz having a skin depth of 9 m and 27 m for 10 Ωm and 100 Ωm formations respectively (see Table 3). A higher frequency could have resolved shallow thin layers. Alternate bands of leached and possible quick clay were interpreted down to 25 m depth below surface and no unleached clay (<10 Ωm) was detected by geotechnical drilling and 2D resistivity survey. This is in the agreement with interpreted resistivity values from FHEM.

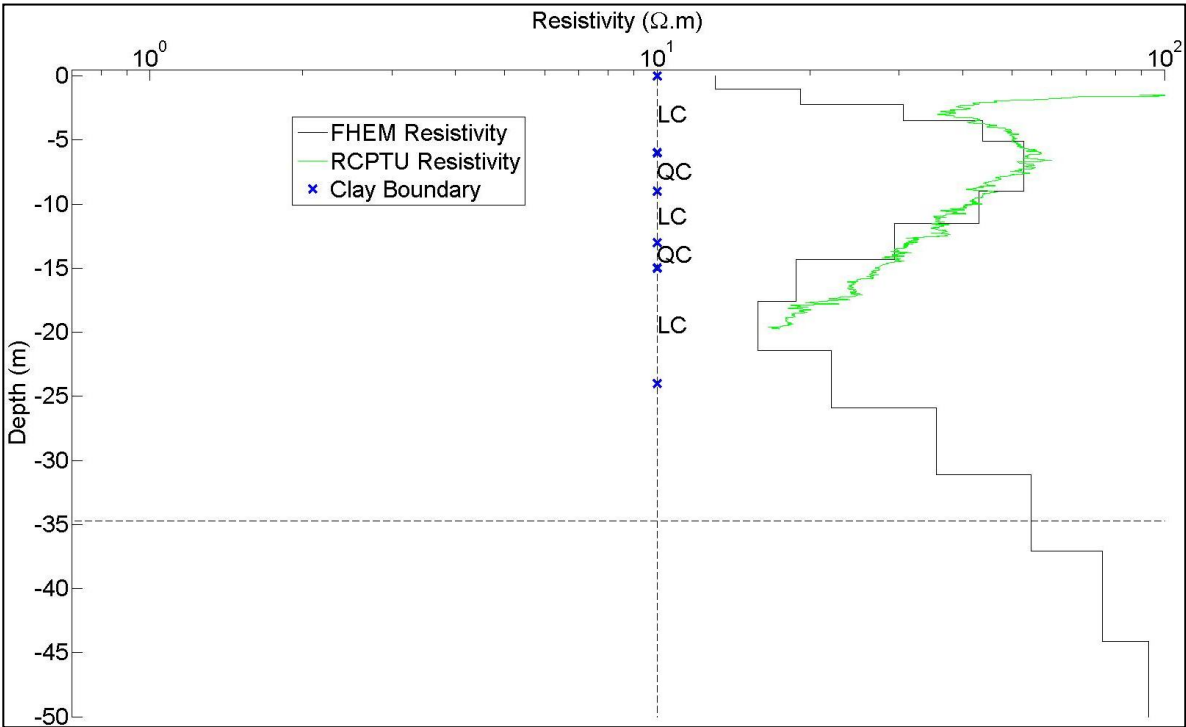


Figure 40: Comparison of FHEM, RCPTu and clay type interpretation near geotechnical drilling point 11 (see table 4 and Fig. 1). Vertical and horizontal dashed lines are unleached-leached clay boundary (10 Ωm) and FHEM DOI, respectively.

Figure 41 shows again good agreement between resistivity values from RCPTu and FHEM. Resistivity values obtained from RCPTu and FHEM are not equal but close and we observe similar trend from both the methods. Leached and possible quick clay were interpreted down to 15 m depth which is in some agreement with observed resistivity values. However, FHEM and RCPTu suggest dropping of resistivity value below 10 Ωm around 12 m and 15 m, respectively to mark it as unleached clay further down.

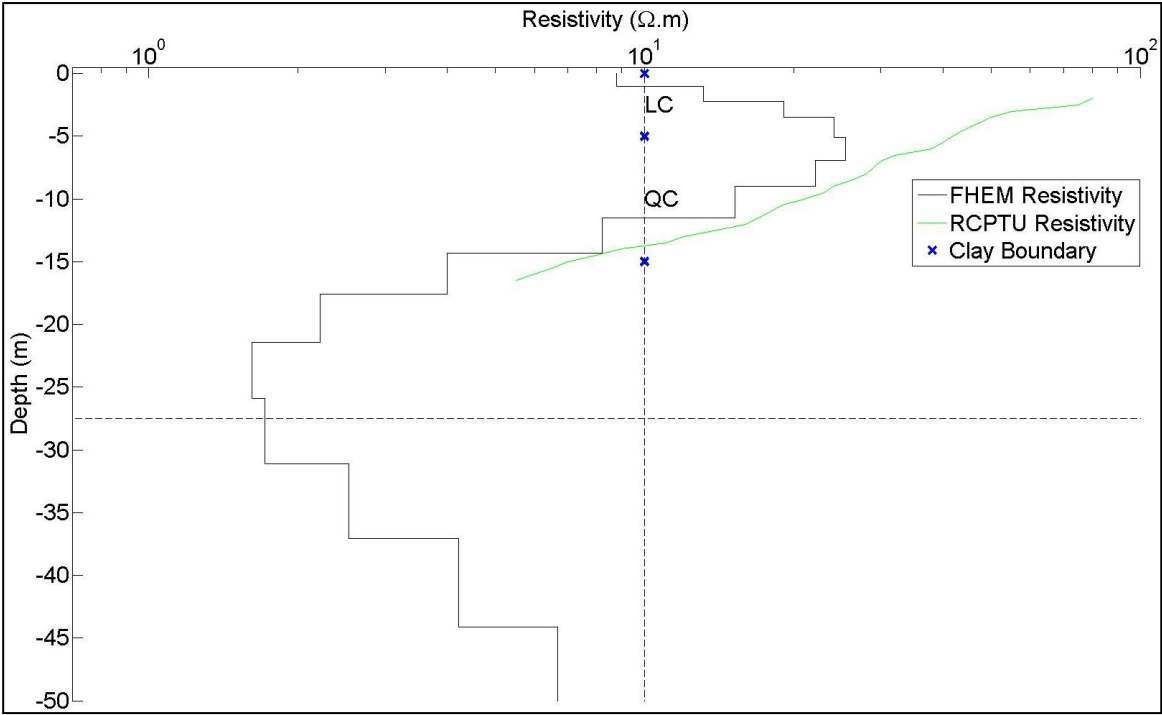


Figure 41: Comparison of FHEM, RCPTu and clay type interpretation near geotechnical drilling point 2 (see table 4 and Fig. 1). Vertical and horizontal dashed lines are unleached-leached clay boundary (10 Ωm) and FHEM DOI, respectively.

At geotechnical drilling locations A and 202, we didn't have RCPTu measurements but they were very close to FHEM and 2D resistivity lines therefore we compared resistivity values obtained from both surveys and shown in Figs. 42 and 43. At location A, FHEM interprets resistivity variation from 2 Ωm to 9 Ωm down to approx. 21 m depth (DOI by FHEM) however 2D resistivity suggests resistivity variation from 10 Ωm to 100 Ωm to similar depth. Clay type interpretation suggests alternate band of leached clay and assumed quick clay down to 30 m depth and unleached clay below it however FHEM resistivity suggest unleached clay to continue from the surface itself. 2D resistivity interpretation is close to the clay type interpretation. At location 202, both FHEM and 2D resistivity survey suggest resistivity < 10 Ωm from the surface to deeper depths and interpreted values are close to each-other. However, a leached clay was interpreted down to 7 m depth and an unleached clay (<10 Ωm) below it from geotechnical drilling results.

We see a good agreement of resistivity values interpreted from FHEM and RCPTu surveys. Agreement between FHEM and 2D ground resistivity survey are not very good but still close enough in the context of the uncertainties associated with such geophysical surveys and inversion methods. It is important to note that FHEM provides an averaged/volumetric resistivity of subsurface however 2D resistivity and especially RCPTu interpret local variations better.

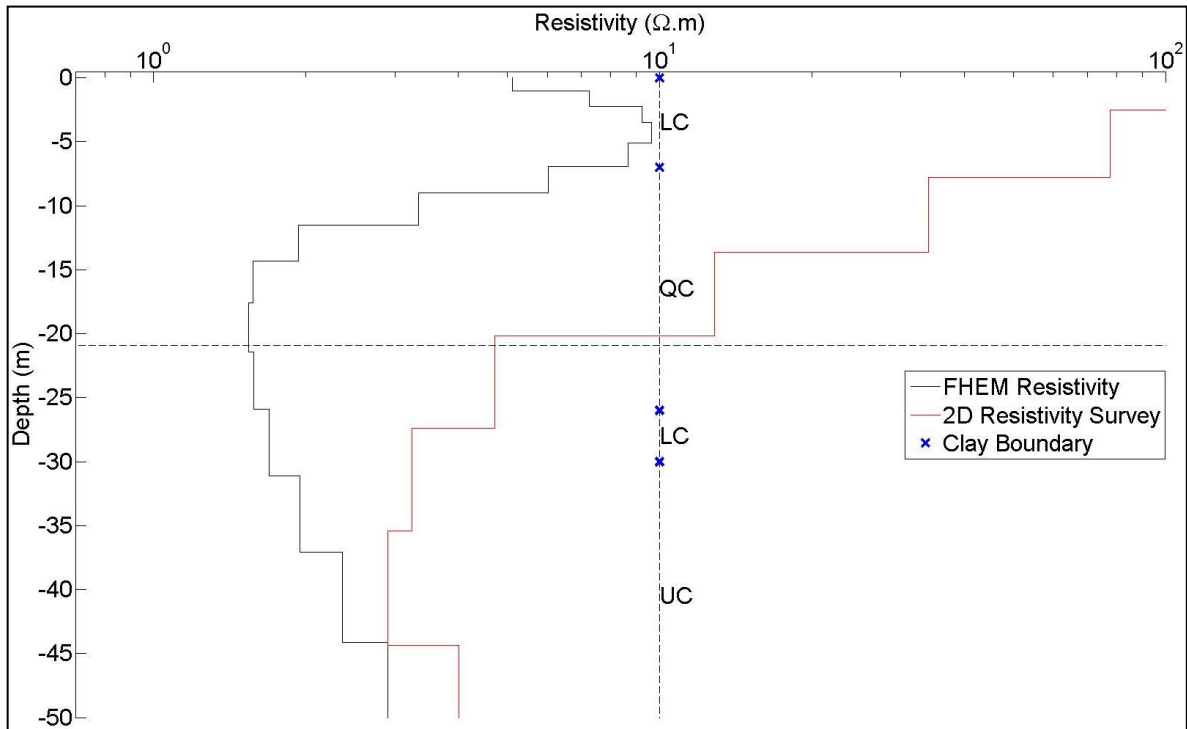


Figure 42: Comparison of FHEM, 2D Resistivity survey and clay type interpretation near geotechnical drilling point A (see table 4 and Fig. 1). Vertical and horizontal dashed lines are un-leached-leached clay boundary (10 Ωm) and FHEM DOI, respectively.

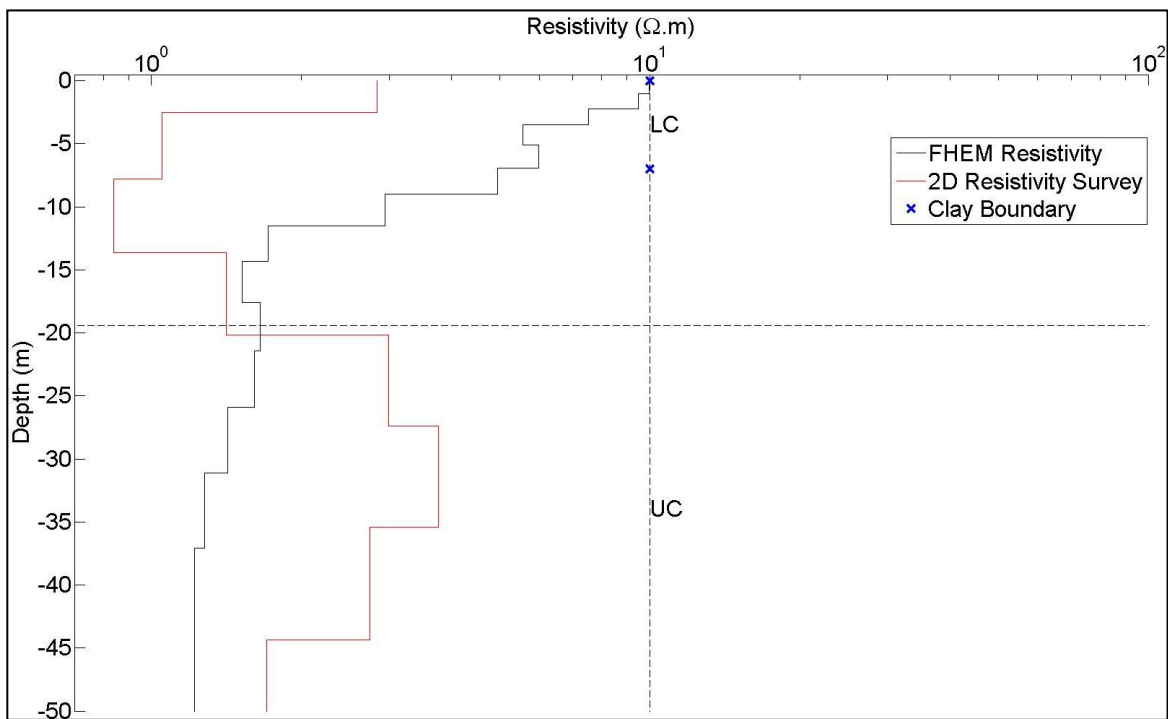


Figure 43: Comparison of FHEM, 2D Resistivity survey and clay type interpretation near geotechnical drilling point 202 (see table 4 and Fig. 1). Vertical and horizontal dashed lines are un-leached-leached clay boundary (10 Ωm) and FHEM DOI, respectively.

4. DISCUSSION

We have observed from our experiences at NGU and from various literatures that the resistivity method is an efficient tool for clay characterization (Solberg et al. 2008, Solberg et al. 2011, Solberg et al. 2015). In this study, we have tested helicopter-borne ElectroMagnetic survey for the same purpose. Comparison of 2D resistivity, refraction seismic and FHEM data interpretation together with exposed bedrock locations suggests that FHEM data can be used for marine sediment mapping and also to show a rough bedrock depth. It can differentiate between layers of unleached marine clay ($< 10 \Omega\text{m}$) and leached marine clay or possible quick clay ($10 - 100 \Omega\text{m}$). However similar resistivity values as those of possible quick clay ($10-100 \Omega\text{m}$), can also suggest non-quick clay and silty sediments. FHEM and 2D ground resistivity inversion suggests bedrock resistivity as low as $200 \Omega\text{m}$ which should be actually several thousands Ωm . It is observed that interpretation of FHEM data including estimation of resistivity and depth down to 20 m underneath very conductive layers is not reliable due to low DOI (Depth Of Investigation) of FHEM data in such areas. We detail the discussion in following subsections.

4.1 Evaluation of inversion codes for FHEM data

Two inversion codes, EM1DFM from UBC and AarhusInv from Aarhus University, are used for inversion of FEEM data. Both the software yields broadly similar conductive models except along few lines where it was very different. AarhusInv is found more appropriate and up-to-date to invert FHEM data with many additional features which EM1DFM does not offer. One of the main advantages of AarhusInv is to perform LCI and SCI which makes the inversion pseudo 2D and 3D instead of simple 1D inversion as available in EM1DFM. DOI calculated from AarhusInv is another very useful feature which tells about the depth extent of the reliable models. We observed that resistivity structures obtained above DOI were independent of starting model and inversion parameters. However, resistivity structures below DOI were changing a lot with different inversion parameters. DOI calculation for present study suggests that only results of approx. 20-40 m depth in highly conductive regions are reliable from FHEM data. Specially constrained inversion of all the FHEM lines using AarhusInv provides a useful 3D model of subsurface resistivity which can be used to plot iso-surface resistivity models, resistivity slices at various depths etc.

4.2 Inverted resistivity levels from 2D resistivity and FHEM data

We compared resistivity obtained from 2D resistivity ground survey and airborne EM survey along four lines. Interpreted resistivity values do not match exactly from these two types of completely independent geophysical methods. The physics behind these methods is also very different. In ground resistivity method, we measure direct current and potential difference in subsurface by direct contact (electrodes), while in electromagnetic method, we measure secondary magnetic field generated due to induced currents. However, basis objective for both of these methods is to interpret subsurface resistivity distribution. Still, we observe broadly similar conductive structures at almost same locations. 2D ground resistivity shows a local variation of resistivity distribution, however, in airborne electromagnetic, resistivity distribution is averaged from a relatively larger area in a volumetric sense.

Comparison of borehole resistivity obtained from RCPTu and subsurface resistivity obtained for 2D resistivity and FHEM survey at very close locations gives further insights about validity of these geophysical methods. A broadly similar resistivity variation but not exact is observed from four locations which supports well the validity of FHEM results.

4.3 Depth to bedrock from FHEM survey

EM method is not well suited for bedrock mapping because we get induced current and a response when there are conductive materials in subsurface. We get very poor response when there are exposed or shallow bedrock in the area. So in a way, these low responses indicate presence of shallow or exposed bedrock. We got bedrock depth confirmation from seismic refraction method along various survey lines, however interpreted models from 2D resistivity and FHEM show only a couple of hundred Ωm resistivity at these locations while we expect in order of thousand Ωm for the bedrock. Reasons for seeing low resistivity in bedrock could be presence of fractured rock and graphite bearing rocks observed in the area. By comparing seismic refraction, 2D resistivity and FHEM results, resistivity of 200 Ωm is assumed as indication of bedrock resistivity. The bedrock depth map made from FHEM data matched well with confirmed bedrock depth by drilling at four locations.

Because a smooth inversion was performed on FHEM data, interpreted resistivity could be a compromise between resistivity of dry clay and bedrock. Smooth inversion also doesn't resolve sharp boundaries therefore this approach of creating bedrock depth from FHEM interpreted resistive values alone could be too simplistic and not accurate. More borehole data and depth confirmation from drilling are needed to cross-check and adapt it for better accuracy.

4.4 Mapping efficiency of airborne survey over ground survey

Main advantage to perform airborne EM survey for such areas is covering a large area in a relatively short time (in this case, less than 5 hours helicopter time) which is not possible at all by ground geophysical measurements like 2D resistivity survey. Airborne EM survey is cost effective if we consider covering a large area by other ground geophysical surveys. The airborne EM survey can be used as first hand tool to look in a large area as reconnaissance survey and to identify interesting zones for a more detailed follow up. Still, we obtained quite detailed information from the FHEM survey in the region.

5. CONCLUSIONS

Various geophysical surveys were performed in a landslide area to investigate marine sediment and possible quick clay deposits. Presence of quick clay can be confirmed only with geotechnical drillings and testing of soil samples. In practise, 2D resistivity survey provides a detailed subsurface resistivity down to approx. one hundred meters of depth which can help in differentiating between leached and unleached clay areas. However, 2D resistivity survey needs more manpower and it is relatively time-consuming. FHEM survey may also provide high resolution subsurface resistivity, however not as detailed as 2D resistivity survey but it can cover a large area in a rather short time (e.g. in few days).

Our FHEM equipment performed measurements at five frequencies with the help of five transmitter-receiver coil pairs namely at 880 Hz, 6606 Hz and 34133 Hz in co-planar setting and 980 Hz and 7001 Hz in co-axial setting. It is an old Hummingbird system and specially designed for mineral prospecting but it still provides useful information about marine clay deposits. The standard FHEM survey should be performed at approx. 30 m bird height above surface in a relatively plain area. The study area in Byneset, Trondheim is not mountainous but due to safety, the pilot could perform the survey at an average bird height of 60 m only which might have reduced efficacy of the collected data. However, having all these limitations, we found a good result from our FHEM data. We could infer some critical information from it and also cross-checked it with RCPTu, 2D resistivity and refraction seismic. We found broadly similar conductive features from FHEM data as shown by 2D ground resistivity data. We could not find a good match for bedrock depth shown by FHEM and refraction seismic. This may be due to limited depth of investigation of FHEM data in conductive overburden areas and presence of conductive minerals in the bedrock. We could see some good correlation in FHEM data results, exposed bedrock observation and depth of confirmed bedrock from drilling. Resistivity obtained from RCPTu at two geotechnical drilling locations matched well with interpreted FHEM resistivity. Resistivity from FHEM and 2D ground resistivity from another two geotechnical drilling locations do not match one-to-one but have shown similar trend.

6. REFERENCES

- AarhusInv, 2013: Manual for inversion program, ver. 6.1, HydroGeophysics Group (HGG), University of Aarhus, Denmark, 71.
http://www.hgg.geo.au.dk/HGGsoftware/em1dinv/em1dinv_manual.pdf
- Abraham J.D., Cannia J.C., Bedrosian P.A., Johnson M.R., Ball L.B., and Sibray S.S., 2012: Airborne electromagnetic mapping of the base of aquifer in areas of western Nebraska: U.S. Geological Survey Scientific Investigations Report, 2011–5219, 38 p.
- Allard M., 2007: On the Origin of the HTEM Species: In "Proceedings of Exploration 07: Fifth Decennial International Conference on Mineral Exploration" edited by B. Milkereit, 355-374.
- Auken, E. and Christiansen A.V. 2004: Layered and laterally constrained 2D inversion of resistivity data: *Geophysics*, 69, 752-761.
- Christiansen A.V. and Auken E. 2012: A global measure for depth of investigation: *Geophysics*, 77, WB171-WB177.
- Christiansen A.V., Auken E., Foged N. and Sørensen K.I. 2007: Mutually and laterally constrained inversion of CVES and TEM data - A case study: *Near Surface Geophysics*, 5, 115-124.
- Dahlin T. 1993: On the Automation of 2D Resistivity Surveying for Engineering and Environmental Applications. Ph.D. Thesis, Department of Engineering Geology, Lund Institute of Technology, Lund University. ISBN 91-628-1032-4.
- Deszcz-Pan M., Fitterman D.V. and Labson V.F. 1998: Reduction of inversion errors in helicopter EM data using auxiliary information: *Exploration Geophysics*, 29, 142–146.
- Farquharson C.G., Oldenburg D.W. and Routh P.S. 2003: Simultaneous 1D inversion of loop-loop electromagnetic data for magnetic susceptibility and electrical conductivity: *Geophysics*, 68, 1857-1869.
- Fugro, 2010: Airborne Magnetic and RESOLVE Survey, Fort Yukon Area, Alaska & Fort Wainwright HEM Lines, Logistics And Processing Report, Job no. 10026 & 10039.
- Geotech, 1997: Hummingbird Electromagnetic System. User's manual. Geotech Ltd.
- Hundal E., 2014: CPTU med målt total sonderingsmotstand – nye muligheter for å detektere kvikkleire? Master Thesis, IBAT, NTNU.
- Kalscheuer T., Bastani M., Donohue S., Persson L., Pfaffhuber A., Reiser F. and Ren Z. 2013: Delineation of a quick clay zone at Smørgrav, Norway, with electromagnetic methods under geotechnical constraints: *Journal of Applied Geophysics*, 92, 121-136.
- Ley-Cooper Y., and Macnae J. 2007: Amplitude and phase correction of helicopter EM data: *Geophysics*, 72, 3, F119–F126.

Ley-Cooper Y., Macnae J., Robb T. and Vrbancich J. 2006: Identification of calibration errors in helicopter electromagnetic (HEM) data through transform to the altitude-corrected phase-amplitude domain: *Geophysics*, 71, 2, G27–G34.

Ley-Cooper Y., Munday, T.J. 2013: Groundwater Assessment and Aquifer Characterisation in the Musgrave Province, South Australia: Interpretation of SPECTREM Airborne Electromagnetic Data, Goyder Institute for Water Research Technical Report Series No. 13/7, Adelaide, South Australia.

Loke M.H. 2010: Res2DInv ver. 3.59.102, Geoelectrical Imaging 2D and 3D, Instruction Manual, Geotomo Software, www.geoelectrical.com

Minsley B.J., Kass M.A., Hodges G. and Smith B.D. 2014: Calibration Multielevation calibration of frequency-domain electromagnetic data: *Geophysics*, 79, E201 – E216.

Minsley B.J., Smith B.D., Hammack R., Sams J.I. and Veloski G. 2012: Calibration and filtering strategies for frequency domain electromagnetic data: *Journal of Applied Geophysics*, 80, 56–66.

Montafia A. 2013: Influence of Physical Properties of Marine Clays on Electric Resistivity and Basic Geotechnical Parameters. Master Thesis, IBAT, NTNU

Reite A.J., Sveian H. and Erichsen E. 1999: Trondheim fra istid til nåtid – landskapshistorie og løsmasser. NGU Gråsteinen 5.

Reynolds J. M. 2011: An Introduction to Applied and Environmental Geophysics. Wiley-Blackwell. Oxford, UK

Sauvin G., Lecomte I., Bazin S., Hansen L., Vanneste M. and L’Heuereux J.-S. 2014: On the integrated use of geophysics for quick-clay mapping: The Hvittingfoss case study, Norway: *Journal of Applied Geophysics*, 106, 1-13.

Siemon B., Christiansen A.V. and Auken E. 2009: A review of helicopter-borne electromagnetic methods for groundwater exploration: *Near Surface Geophysics*, 2009, 629-646

Solberg I.L., Dalsegg E., L’Heuereux J.-S. and Rønning J.S. 2012a: Resistivitetsmålinger for løsmassekartlegging ved skredgrop på Byneset, Sør-Trøndelag: NGU report No. 2012.004.

Solberg I.L., Baranwal V.C., Dalsegg E., Dretvik H., Gasser D., Rønning, J.S. and Tønnesen, J.F. 2015: Geologi på Byneset: en sammenstilling av geologiske, geofysiske og geotekniske data, NGU report 2015.002

Solberg I.-L., Hansen L., Rønning J.S., Haugen E.D., Dalsegg E. and Tønnesen J.F. 2012b: Combined geophysical and geotechnical approach to ground investigations and hazard

zonation of a quick clay area, mid Norway: *Bulletin of Engineering Geology and the Environment*, 71, 119-133.

Solberg I.L., Hansen L., Rønning J.S. & Dalsegg E. 2011: Veileder for bruk av resistivitetsmålinger i potensielle kvikkleireområder: Versjon 1.0. NGU rapport 2010.048

Solberg I.L., Rønning J.S., Dalsegg E., Hansen L., Røkoengen K. and Sandven R. 2008: Resistivity measurements as a tool for outlining quick-clay extent and valley-fill stratigraphy: a feasibility study from Buvika, central Norway. *Canadian Geotechnical Journal*. 45, 210–225.

UBC 2000: Manual for running the program "EM1DFM", ver. 1.0, University of British Columbia (UBC), Canada.
<http://www.eos.ubc.ca/ubcgif/iag/sftwrdocs/em1dfm/em1d-man.html>

Valleau N.C. 2000: HEM data processing - a practical overview. *Exploration Geophysics*, 31, 584-594.

Whitehead N. 2005: Helicopter electromagnetic data processing, analysis and presentation system for Oasis montaj v. 6.2, Geosoft HEM system tutorial and user guide, 54.



GEOLOGICAL
SURVEY OF
NORWAY

· NGU ·

Geological Survey of Norway
PO Box 6315, Sluppen
N-7491 Trondheim, Norway

Visitor address
Leiv Eirikssons vei 39
7040 Trondheim

Tel (+ 47) 73 90 40 00
E-mail ngu@ngu.no
Web www.ngu.no/en-gb/